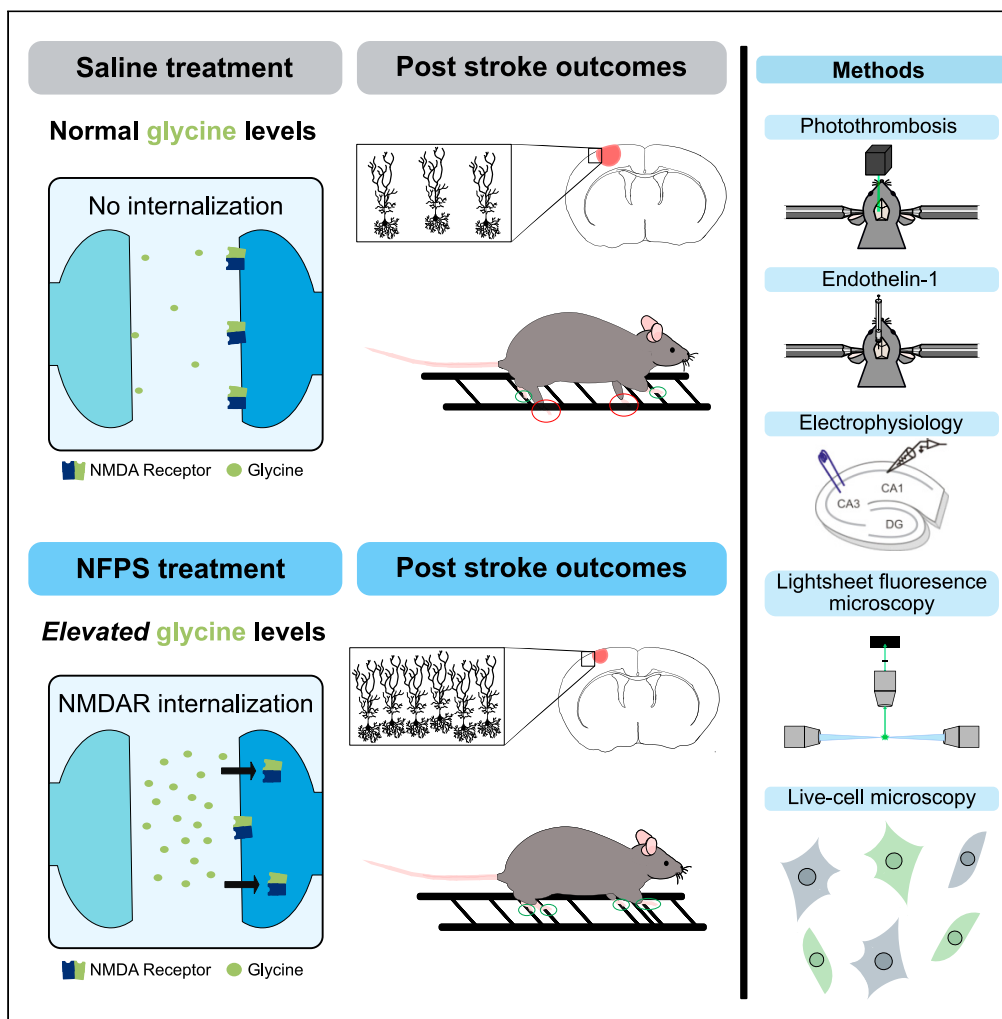


Article

Glycine-induced NMDA receptor internalization provides neuroprotection and preserves vasculature following ischemic stroke



Julia Cappelli,
Pamela Khacho,
Boyang Wang, ...,
Prakash
Chudalayandi,
Adrian Y.C. Wong,
Richard Bergeron

jcapp082@uottawa.ca (J.C.)
rbergeron1003rb@icloud.com
(R.B.)

Highlights
GINI is a dynamic phenomenon which dampens NMDAR-mediated excitotoxicity during stroke

GlyT1-antagonists (GlyT1-As) trigger GINI during stroke *in vivo*

GlyT1-As mitigate post-stroke behavioral deficits and preserve peri-infarct vasculature

GlyT1 could be a novel and viable therapeutic target for ischemic stroke

Cappelli et al., iScience 25, 103539
January 21, 2022 © 2021 The Authors.
<https://doi.org/10.1016/j.isci.2021.103539>



Article

Glycine-induced NMDA receptor internalization provides neuroprotection and preserves vasculature following ischemic stroke

Julia Cappelli,^{1,4,5,*} Pamela Khacho,^{1,4} Boyang Wang,¹ Alexandra Sokolovski,¹ Wafae Bakkar,² Sophie Raymond,¹ Nina Ahlskog,¹ Julian Pitney,¹ Junzheng Wu,¹ Prakash Chudalayandi,¹ Adrian Y.C. Wong,¹ and Richard Bergeron^{1,3,*}

SUMMARY

Ischemic stroke is the second leading cause of death worldwide. Following an ischemic event, neuronal death is triggered by uncontrolled glutamate release leading to overactivation of glutamate sensitive N-methyl-D-aspartate receptor (NMDAR). For gating, NMDARs require not only the binding of glutamate, but also of glycine or a glycine-like compound as a co-agonist. Low glycine doses enhance NMDAR function, whereas high doses trigger glycine-induced NMDAR internalization (GINI) *in vitro*. Here, we report that following an ischemic event, *in vivo*, GINI also occurs and provides neuroprotection in the presence of a GlyT1 antagonist (GlyT1-A). Mice pretreated with a GlyT1-A, which increases synaptic glycine levels, exhibited smaller stroke volume, reduced cell death, and minimized behavioral deficits following stroke induction by either photothrombosis or endothelin-1. Moreover, we show evidence that in ischemic conditions, GlyT1-As preserve the vasculature in the peri-infarct area. Therefore, GlyT1 could be a new target for the treatment of ischemic stroke.

INTRODUCTION

Ischemic stroke is a devastating health concern that often leaves victims with long-lasting disabilities, and induces substantial socioeconomic costs for the individual, their loved ones and society as a whole. Limited effective interventions are available to the at-risk population, highlighting the need to identify novel therapeutic targets that can prevent neuronal death following ischemic insults.

Activity-dependent changes in N-methyl-D-aspartate receptor (NMDAR)-mediated synaptic strength are of great importance, because they serve as the molecular trigger for synaptic responses in many physiological and pathological processes such as ischemic stroke. Neuronal death following an ischemic event is triggered by uncontrolled glutamate release leading to the NMDAR overactivation on surrounding neurons, inducing excessive Ca^{2+} -influx primarily through NMDARs (Wu and Tymianski, 2018). In physiological conditions, NMDARs require glutamate binding on the GluN2 subunit and glycine binding on the glycine binding site (GBS) on the GluN1 subunit (Rosenmund et al., 1998). Ascher's group showed that glycine (Johnson and Ascher, 1987), or a glycine-like substance (Kleckner and Dingledine, 1988), is a required co-agonist for NMDAR activation. Moreover, Salter and co-workers reported that high doses of glycine trigger GINI, *in vitro*, by promoting endocytosis of NMDAR through clathrin/dynamin-dependent machinery (Nong et al., 2003). Unlike constitutive internalization, which requires no channel activation (Nong et al., 2003; Nong et al., 2004), NMDAR internalization following glycine "priming" requires both glutamate and glycine present in the synaptic cleft⁵.

Using a multidisciplinary approach, we found that during an oxygen-glucose deprivation paradigm (OGD), *in vitro*, not only glutamate but also an excess of glycine is released in the extracellular space. However, this is not sufficient to trigger GINI because the level of extracellular glycine is buffered by the glycine transporter type 1 (GlyT1) (Aragon et al., 1987; Guastella et al., 1992; Smith et al., 1992; Bergeron et al., 1998). Only when GlyT1s are antagonized, can glycine accumulate in the synaptic cleft and lead to robust NMDAR internalization. Photothrombosis (PT) and endothelin-1 (ET-1) are paradigms that mimic ischemic

¹Cellular and Molecular Medicine Department, University of Ottawa, 451 Smyth Road, Roger Guindon Building, Room 3501N, Ottawa, ON K1H 8M5, Canada

²Ottawa Hospital Research Institute, 451 Smyth Road, Roger Guindon Building, Room 3501N, Ottawa, ON K1H 8M5, Canada

³Present address: 1600 Carling Ave, Suite 100, Ottawa, ON K1Y 1B2, Canada

⁴These authors contributed equally

⁵Lead contact

*Correspondence:
japp082@uottawa.ca (J.C.),
rbergeron1003rb@icloud.com (R.B.)

<https://doi.org/10.1016/j.isci.2021.103539>



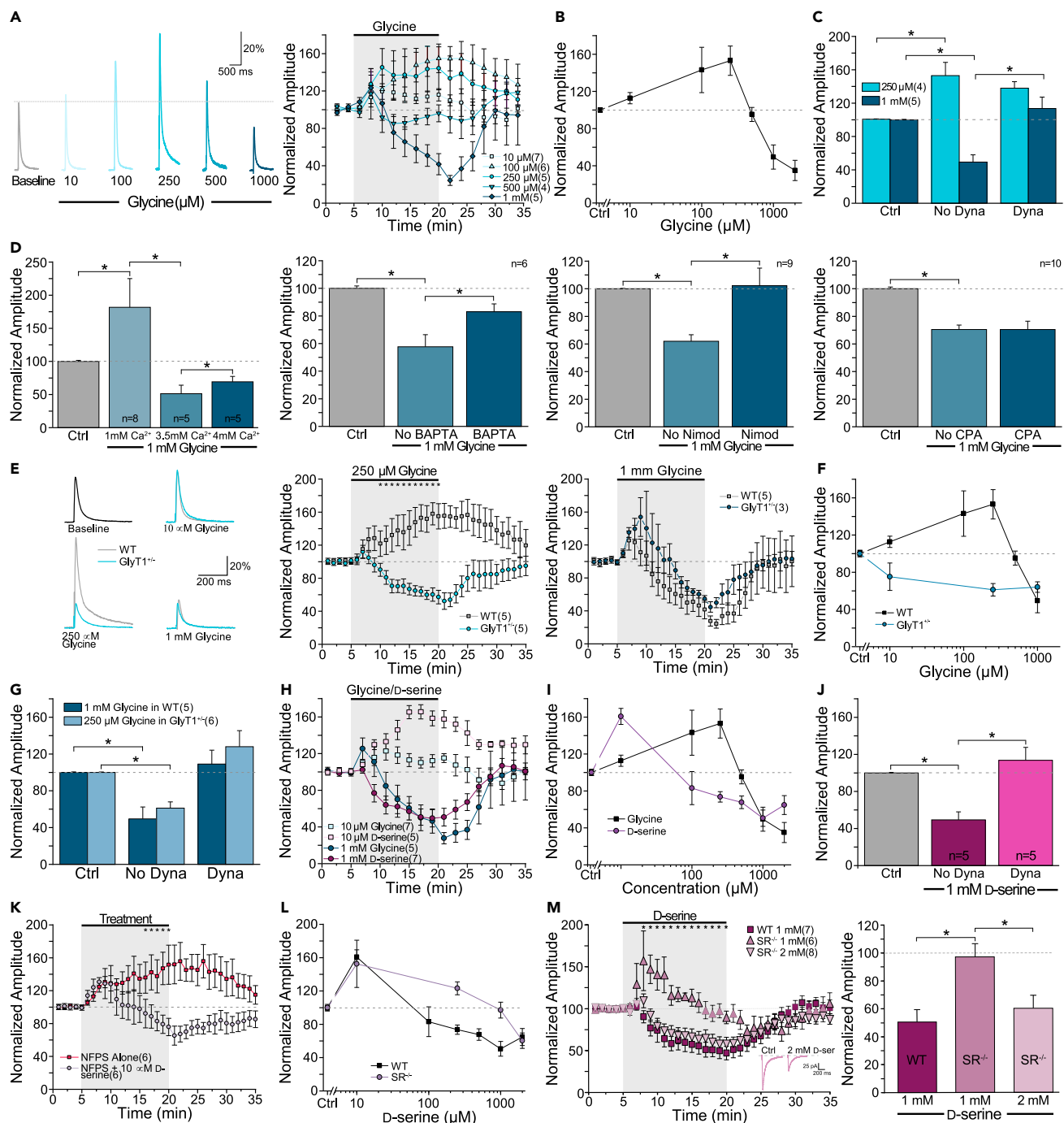


Figure 1. Increasing exogenous glycine and D-serine concentrations results in NMDAR internalization, which is dependent on Ca^{2+} influx

- (A) Normalized raw traces showing the effect of increasing concentrations of exogenous glycine on Schaffer Collateral NMDAR-EPSCs and mean time course data showing the effect of a 15 mins application of various glycine concentrations.
- (B) A dose-response curve of glycine and NMDAR-EPSC amplitudes.
- (C) The effect of 250 μ M and 1 mM glycine on NMDAR-EPSC amplitudes in the presence of a dynasore.
- (D) The role of various concentrations of extracellular Ca^{2+} on NMDAR-EPSC amplitudes in the presence of 1 mM glycine, as well as changing intracellular Ca^{2+} levels using BAPTA, nimodipine, or CPA.
- (E) The effect of various concentrations of glycine on NMDAR-EPSC amplitudes in GlyT1 $^{+/+}$ mice, compared to WT.
- (F) The dose-response curve of the effects of glycine on NMDAR amplitudes in GlyT1 $^{+/+}$ mice.
- (G) The effect of 250 μ M glycine on NMDAR-EPSC amplitudes in GlyT1 $^{+/+}$ mice in the presence of dynasore.

Figure 1. Continued

- (H) The effect of low (10 μ M) and high (1 mM) concentrations of glycine or D-serine concentrations on NMDAR-EPSC amplitudes.
- (I) The dose-response curve of NMDAR-EPSC amplitudes to D-serine compared to glycine.
- (J) The effect of 1 mM D-serine in the presence of dynasore.
- (K) The effect of 10 μ M D-serine while elevating endogenous glycine levels with NFPS.
- (L) A dose-response curve showing the effect of exogenous D-serine levels on SR $^{−/−}$ mice.
- (M) The effect of a higher dose of D-serine (1 mM vs. 2 mM) on NMDAR-EPSC amplitudes in SR $^{−/−}$ mice compared to their WT littermates. Data is mean \pm SEM; statistical significance $p < 0.05$ *.

events, *in vivo*. We report that both PT and ET-1 induced a significantly smaller stroke volume, less cell death and less behavioral deficits in mice in the presence of a GlyT1 antagonist (GlyT1-A), which increases glycine concentrations, and hence the occupancy of the GBS. Moreover, the neuroprotective effect induced by high occupancy of the GBS was further supported by preservation of the vascularization tree.

Overall, these data suggest that increased levels of synaptic glycine before an ischemic event may be a means of minimizing neuronal death. We report that GlyT1-A administration before or shortly after an ischemic event, *in vivo*, triggers GINI and provides neuroprotection.

RESULTS

High concentrations of glycine induce NMDAR internalization

We first determined the effects of bath application of increasing glycine concentrations on stimulation-evoked NMDAR excitatory postsynaptic currents (NMDAR-EPSCs) recorded from CA1 pyramidal neurons from acute hippocampal brain slices (Figure 1A). At glycine concentrations below 250 μ M, NMDAR-EPSC amplitudes were potentiated in a dose-dependent fashion (Johnson and Ascher, 1987; Bergeron et al., 1998; Forsythe et al., 1988; Paoletti et al., 1995). However, increasing the glycine concentration to 1 mM resulted in a significant decrease in NMDAR-EPSC amplitude (Nong et al., 2003; Han et al., 2013) and this effect was reversible (Figure 1B). To verify that this decrease in amplitude was because of GINI, we applied 1 mM glycine in the presence of 100 μ M dynasore, a cell-permeable inhibitor of both dynamin-1 and dynamin-2, which blocks internalization (Nong et al., 2004; Kirchhausen et al., 2008). We found that the decrease in NMDAR-EPSC amplitudes by 1 mM glycine was abolished in the presence of dynasore (Figure 1C).

Calcium influx is required for GINI to occur

Previous studies have reported that the activity of dynamin is regulated by the Ca^{2+} -sensitive phosphatase calcineurin (Lai et al., 1999; Traynelis et al., 2010). Therefore, we explored the role of extracellular and intracellular Ca^{2+} on NMDAR-EPSC amplitudes in the presence of 1 mM glycine. We examined the effects of various external Ca^{2+} concentrations on the NMDAR response to 1 mM glycine application. When 1 mM glycine was applied with low Ca^{2+} (1 mM), an increase in NMDAR-EPSC amplitude was observed, in contrast to what occurred with normal Ca^{2+} concentrations (3.5 mM). To further confirm the role of Ca^{2+} in GINI, we included a Ca^{2+} -chelator BAPTA (10 mM), in the recording electrode. Here, we observed a significant attenuation in the decrease in NMDAR-EPSC amplitude induced by 1 mM exogenous glycine. Moreover, extracellular application of 20 μ M nimodipine, a L-type Ca^{2+} channel blocker, also attenuated GINI compared to control, further corroborating the data acquired with BAPTA. In contrast, depleting intracellular Ca^{2+} stores by incubating hippocampal slices for 1 hr in 30 μ M cyclopiazonic acid (CPA), an inhibitor of intracellular Ca^{2+} pumps, had no effect on the glycine-induced decrease in NMDAR-EPSC amplitude (Figure 1D). Together these data suggest that external Ca^{2+} influx across the plasma membrane is required for GINI to occur.

Genetic elevation of extracellular glycine facilitates GINI

Heterozygous glycine transporter type 1 (GlyT1 $^{+/−}$) mice exhibit a higher level of endogenous extracellular glycine (Gomeza et al., 2003; Tsai et al., 2004). Therefore, we hypothesized that in these mice GINI could be triggered by lower doses of glycine. As illustrated in Figure 1E, although there was no significant effect in the NMDAR-EPSC amplitude following bath application of 10 μ M or 1 mM glycine between wild type (WT) and GlyT1 $^{+/−}$ mice, bath application of 250 μ M glycine, which potentiated the NMDAR-EPSC amplitude in WT mice, significantly inhibited the NMDAR-EPSC amplitude in GlyT1 $^{+/−}$ mice (Figure 1F). The decrease of the NMDAR-EPSC amplitude induced by 250 μ M glycine in GlyT1 $^{+/−}$ mice was abolished in the presence

of dynasore (Figure 1G). Therefore, the high levels of endogenous glycine in the GlyT1^{+/−} mice trigger GINI at lower exogenous glycine concentrations.

Role of glycine binding site occupancy

In addition to glycine, D-serine also activates the GBS (Kleckner and Dingledine, 1988; Papouin et al., 2012). As illustrated in Figure 1H, the effects of increasing D-serine concentrations on NMDAR-EPSC amplitudes in acute slices from WT mice was also dose-dependent. Moreover, the dose-response curve of NMDAR-EPSC amplitudes to D-serine was left-shifted relative to that of glycine because of its higher affinity to the GBS (Wolosker et al., 1999) (Figure 1I). The decrease in NMDAR-EPSC amplitude evoked following bath application of 1 mM D-serine was also abolished in the presence of dynasore (Figure 1J).

We next investigated whether GINI could be modulated by increasing levels of either glycine or D-serine in WT mice. Glycine levels were increased via bath application of the selective GlyT1-A, N-[3-(4'-fluorophenyl)-3-(4'-phenylphenoxy)propyl]sarcosine (NFPS; 300 nM) (Aubrey and Vandenberg, 2001; Herdon et al., 2001; Mallorga et al., 2003; Liu et al., 2005; Pinto et al., 2015). As expected, there was a significant increase in evoked NMDAR-EPSC amplitude in the presence of NFPS alone (Bergeron et al., 1998). However, when NFPS was applied together with a potentiating concentration of D-serine (10 μM), a significant decrease in NMDAR-EPSC amplitude was observed (Figure 1K). Interestingly, when NMDARs were first primed with high doses of glycine or D-serine, a subsequent application of a low dose of glycine or D-serine, also induced GINI (Figure S1).

Next, we used a transgenic mouse model in which the serine racemase gene was knocked out (SR^{−/−} mice) (Basu et al., 2009; Balu et al., 2012; Benneyworth and Coyle, 2012), as these mice exhibit low levels of D-serine. In both WT and SR^{−/−} mice, a low dose of D-serine (10 μM) potentiated the evoked NMDAR-EPSC amplitude. However, SR^{−/−} mice required a higher dose of D-serine (2 mM) than WT mice (1 mM) to induce a decrease in NMDAR-EPSC amplitude (Figures 1L and 1M). These findings suggest that there is a common mechanism of action for glycine or D-serine to trigger GINI. In addition, we found that GINI was neither sub-unit-specific (Figures S2A–S2E) nor attributed to AMPA receptor activity (Figure S2F), and not limited to the hippocampal region (Figure S2G).

Glycine is released during oxygen-glucose deprivation

Immunohistochemical data suggests that glycine may be co-localized in glutamatergic neurons (Cubelos et al., 2005); therefore, we hypothesized that depolarization of glutamatergic CA1 pyramidal neurons during the oxygen-glucose deprivation (OGD) paradigm could result in detectable local glycine release (Rossi et al., 2007). To ensure glycine was released during an OGD paradigm, we used the sniffer-patch technique, wherein activation of glycine receptor α2 subunit indicated glycine release (Muller et al., 2013). When the OGD perfusate was applied to the slice, there was a marked increase in the frequency of channel opening in the patch (Figure S3A) and a significant increase in open probability (P_{open}) compared to control (Figure S3B). Overall, these results strongly suggest that during OGD conditions, glycine is released into the CA1 extracellular space. Given that multiple studies have demonstrated that glycine receptors (GlyRs) are only weakly expressed at CA1 hippocampal synapses (Muller et al., 2013; Hu et al., 2016; Chen et al., 2015), we speculated that the target for the glycine release following OGD could be NMDARs.

OGD paradigm on acute slices, *in vitro*, decreases NMDAR current amplitude

In brief, we found that an OGD paradigm applied to acute slices during train stimulation induced NMDAR internalization (Figures S3C–S3G). To further confirm that glycine is responsible, we purified glycine oxidase (GO), an enzyme that catalyzes the breakdown of glycine. After demonstrating the effectiveness of purified GO on exogenous glycine levels (Figure S3H), NMDAR-EPSC trains (20 Hz) were recorded with GO and the decrease of the NMDAR-EPSC amplitude was abolished following OGD (Figures S3I and S3J). Altogether, these *in vitro* data demonstrate that glycine levels increase during ischemia; however, GINI is only triggered when we further elevate glycine using the train stimulation paradigm. Therefore, we speculated that GINI could also be triggered *in vivo* during stroke in mice with elevated glycine levels.

Genetic elevation of brain glycine reduces infarct size following photothrombosis

Glycine has been shown to be neuroprotective in both *in vitro* (Hu et al., 2016) and *in vivo* models of stroke (Chen et al., 2015, 2017; Zhao et al., 2018; Qin et al., 2019); yet, proposed mechanisms have never been

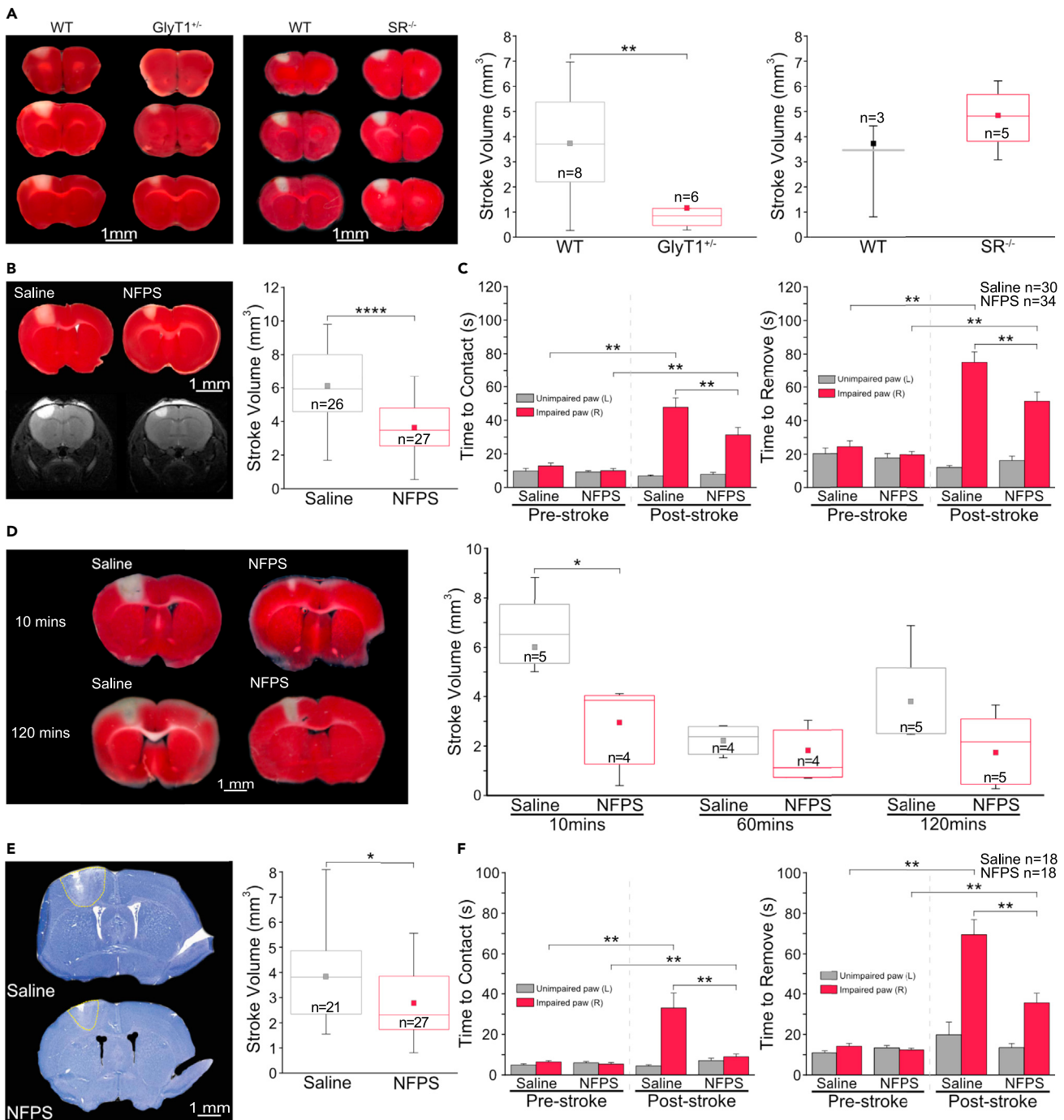


Figure 2. Elevation of extracellular glycine results in a smaller infarct volume and decreased motor behavioral deficits following photothrombotic and endothelin-1 stroke

(A) Representative serial coronal sections of TTC-stained mouse forebrain (slice thickness 500 μ M) and their corresponding box and whisker plots showing the infarct volume when assessed 48hrs after the induction of a unilateral photothrombotic stroke in GlyT1^{+/-} and SR^{-/-} mice relative to WT mice.

(B) Representative TTC-stained (top) or magnetic resonance imaging (bottom) sections showing representative stroke regions observed 48hrs following the induction of photothrombotic (PT) stroke, and a box and whisker plot showing stroke volume in saline-treated or NFPS-treated mice 24hrs before stroke induction.

(C) The effect of 24hrs pre-stroke NFPS administration on post-stroke time to contact and time to remove in the adhesive removal task compared with saline treatment, when evaluated 48hrs following PT stroke.

Figure 2. Continued

(D) Effect of various post-stroke administration time-points of NFPS treatment on stroke volume with their corresponding box and whisker plots following PT stroke.

(E) Representative cresyl violet sections (25 μ m thick) 48hrs following endothelin-1 (ET-1) stroke obtained from saline-treated and NFPS-treated mice 24hrs prior, in which the extent of the infarct is shown within the yellow border and box and whisker plot depicting infarct volume.

(F) The effect of 24hrs pre-stroke NFPS administration on post-stroke time to contact and time to remove in the adhesive removal task compared with saline treatment following ET-1 stroke. Data is mean \pm SEM; statistical significance $p < 0.05^*$, $p < 0.01^{**}$, $p < 0.001^{***}$, and $p < 0.0001^{****}$

expanded into feasible pharmacotherapies. To determine if high glycine levels could result in a decrease in neuronal death following ischemia, we used a well-established focal ischemic paradigm, photothrombosis (PT). Because our *in vitro* data demonstrate that high glycine/D-serine levels are required to trigger GINI, one would expect that the stroke volume in GlyT1^{+/−} mice should be smaller than that observed in WT mice. Indeed, there was a statistically significant decrease in stroke volume in the GlyT1^{+/−} mice compared to WT. In contrast, stroke volumes were larger in SR^{−/−} mice, compared to WT (Figure 2A).

Pharmacological elevation of brain glycine reduces infarct size following photothrombosis

To acutely increase the levels of endogenous glycine, WT mice were treated with NFPS 24hrs pre-stroke (Aubrey and Vandenberg, 2001; Herdon et al., 2001; Mallorga et al., 2003; Liu et al., 2005). Forty-eight hours following PT stroke in both the saline- and NFPS-treated cohorts, stroke volume was quantified using 2,3,5-triphenyltetrazolium chloride (TTC) or via magnetic resonance imaging (MRI). The box-and-whisker plot shows a statistically significant decrease in median stroke volume in the NFPS-treated mice compared to the saline-treated mice (Figure 2B). This decrease in infarct volume following NFPS treatment is consistent with what has been previously observed in the transient middle cerebral artery occlusion (tMCAO) model of ischemic stroke (Huang et al., 2016; Dojo Soeandy et al., 2019). In addition, FluoroJade C (FJC) staining demonstrated that the NFPS-treated mice also have significantly decreased levels of cell death compared with the saline-treated mice (Figure S4A). Therefore, these data demonstrate that the blockade of GlyT1 is required for the reduction of stroke volume. Interestingly, this decrease in stroke volume was maintained when NFPS was administered up to 10mins post-stroke (Figure 2D).

Pharmacological elevation of brain glycine minimizes motor behavioral deficits following photothrombosis

Although encouraging, a decrease in stroke volume does not necessarily correlate with a decrease in post-stroke behavioral deficits (Pineiro et al., 2000). To determine if pre-treatment with NFPS could minimize post-stroke behavioral deficits, we used a well-established behavioral test of motor function, the adhesive removal test (Bouet et al., 2009). Following PT, a significant attenuation of post-stroke motor behavioral deficits was observed in the cohort of mice treated with NFPS in both time to contact and time to remove, with no significant stroke or drug effect on the unimpaired paw (Figure 2C).

Pre-stroke administration of NFPS decreases stroke volume and improves motor behavioral deficits following endothelin-1 stroke

The PT stroke model does not recapitulate all of the clinical aspects of ischemia, particularly with respect to reperfusion of the infarct (Sommer, 2017). Therefore, to ensure that the observed decrease in stroke volume and attenuation of behavioral deficits was not an artifact of the PT stroke model, we repeated the experiments using a second known model of focal stroke, the endothelin-1 (ET-1) model (Dojo Soeandy et al., 2019). Mice pre-treated with NFPS had significantly smaller ET-1 stroke volumes compared with their saline-treated counterparts (Figure 2E).

In the adhesive removal task, NFPS-treated mice showed significantly less post-stroke impairments in the impaired paw than the saline-treated mice, in both time to contact and time to remove (Figure 2F). There was no significant stroke or drug effect on the unimpaired paw (Supplementary adhesive and cylinder task (Schallert et al., 2000) data for both stroke models in Figures S4B–S4E and validation of ET-1 model in Figures S5A–S5C). The horizontal ladder test was an additional assessment of motor function (Metz and Whishaw, 2009). Following ET-1 stroke, there was a significant increase in impaired paw misses in the saline-treated group; however, in the NFPS-treated group, no significant increase in misses was observed (Figures S4F and S4G). These data demonstrate that the blockade of GlyT1 ameliorated post-stroke outcomes in two models of stroke. Furthermore, this effect was not because of hypothermia (Figure S5E).

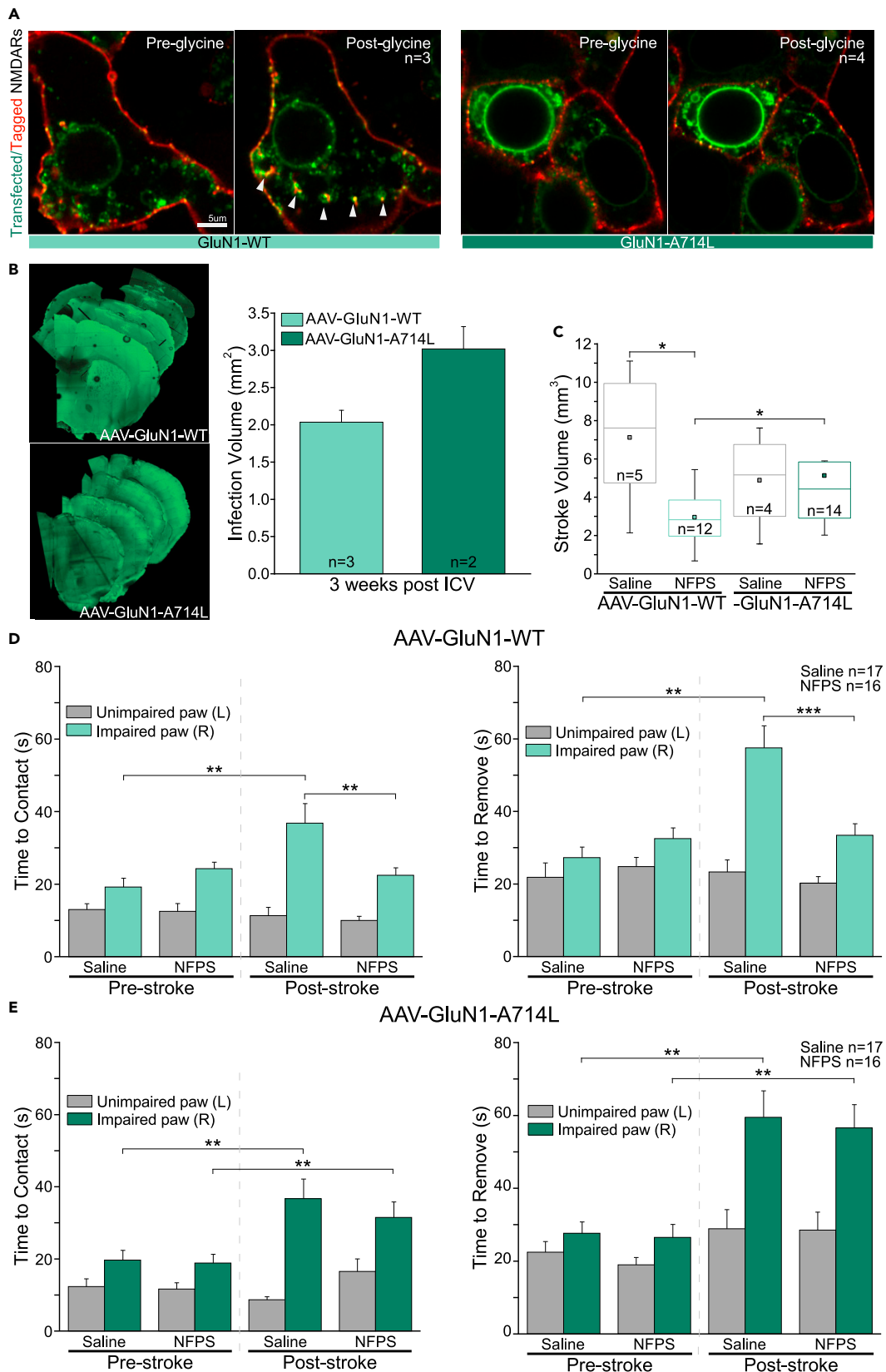


Figure 3. Infection of the stroke site with the non-internalizing GluN1-A714L mutation abolishes the protective effect of elevating extracellular glycine on stroke volume and during a behavioral task

(A) Visual representation of NMDAR internalization in GluN1-WT or GluN1-A714L transfected HEK293 cells following application of 1 mM glycine. Transfected NMDARs are labeled in green, whereas extracellular NMDARs are additionally labeled with red cell impermeable nanobody staining.

(B) Representative images showing the extent of viral spread in the mouse forebrain following infection between mice infected with AAV-GluN1-WT or AAV-GluN1-A714L.

(C) Box and whisker plot showing the effect of NFPS administration 24hrs before PT stroke induction in mice infected with AAV-GluN1-WT or AAV-GluN1-A714L.

(D and E) The effect of NFPS on post-stroke time to contact and time to remove in the adhesive removal task compared with saline treatment, in mice infected with AAV-GluN1-WT (D), and in mice infected with AAV-GluN1-A714L (E) 48hrs following PT stroke. Data is mean \pm SEM; statistical significance $p < 0.05 ^*$, $p < 0.01 **$, and $p < 0.001 ***$.

Therefore, these data emphasize the crucial role of GlyT1-A in the observed neuroprotection, and this is likely occurring because of GINI.

Blocking NMDAR internalization abolishes the neuroprotective effect of NFPS on stroke volume and behavior

GINI is driven by the recruitment of AP-2 and is mediated by A714 on the C-terminal domain of GluN1. Glycine priming for internalization is specific to A714; therefore, this residue is necessary for priming of NMDARs containing either GluN2A or GluN2B in recombinant systems (Han et al., 2013). To confirm that our *in vivo* observations are because of GINI, we introduced a point mutation into the NMDAR GluN1 subunit (A714L), which abolishes glycine-mediated NMDAR internalization *in vitro* (Han et al., 2013). We first assessed the functionality of the mutation via transient transfection of GluN1-WT or GluN1-A714L together with WT GluN2A subunit into HEK293 cells resulting in a functional NMDAR. Application of 1 mM glycine in cells expressing GluN1-WT induced a significant decrease in the amplitude of the NMDAR-EPSC, whereas in cells expressing GluN1-A714L this concentration significantly increased the NMDAR amplitude (Figures S6A and S6B). To visually confirm that GINI was occurring, the movements of NMDARs were tracked over time by live-cell imaging following application of 1 mM glycine (Figures 3A and S6C; Videos S1 and S2).

This GluN1 viral construct was then packaged into an adeno-associated virus (AAV) 2/9 and injected into the sensory-motor cortex of mice. The overall function of the NMDARs was reassessed in acute slices. A dose of 1 mM glycine did not decrease NMDAR-EPSC amplitudes in cells infected with the AAV-GluN1-A714L constructs (Figure S6D). The spread of the virus occupied a volume that was comparable to the PT stroke (Figures 3B and S7A), and there were no significant differences in the PT-induced stroke volume between the mice infected with either the AAV-GluN1-WT or the AAV-GluN1-A714L constructs (Figure 3C). However, there was a significant decrease in stroke volume following pre-treatment with NFPS in mice infected with AAV-GluN1-WT. NFPS administration had no effect on stroke volume in the mice infected with AAV-GluN1-A714L.

The adhesive removal test was repeated on mice infected with either the AAV-GluN1-A714L mutation or the AAV-GluN1-WT. Administration of NFPS to the mice infected with AAV-GluN1-WT resulted in a significant decrease in post-stroke time to contact and time to remove in the impaired paw (Figure 3D). Interestingly, in mice infected with the AAV-GluN1-A714L (Figure 3E), there was no significant change in time to contact and time to remove following stroke in the NFPS-treated mice. Data illustrated in Figure S5D confirm that the injections of the AAV-GluN1-WT or -GluN1-A714L alone had no effect on behavior. Taken together, these data confirm that GlyT1-A administration induces neuroprotection *in vivo*, via GINI.

Pre-stroke administration of NFPS attenuates vascular dysfunction

Stroke is primarily characterized as a vascular disease; therefore, we evaluated the impact of NFPS on vascular function and morphology following PT stroke. Using Laser Doppler flowmetry (LDF), we found that PT stroke induced a significant decrease in blood flow and this effect was rescued with NFPS pre-treatment (Figure 4A). In GlyT1^{+/−} mice, there was no significant change in blood flow following stroke. Interestingly, in SR^{−/−} mice, PT stroke induced a highly significant decrease in blood flow (Figure 4B).

We next assessed if NFPS could modify vascular morphology by pairing transcardial perfusions of a fluorescent dye with tissue clearing and light sheet fluorescence microscopy (LSFM). This strategy allowed

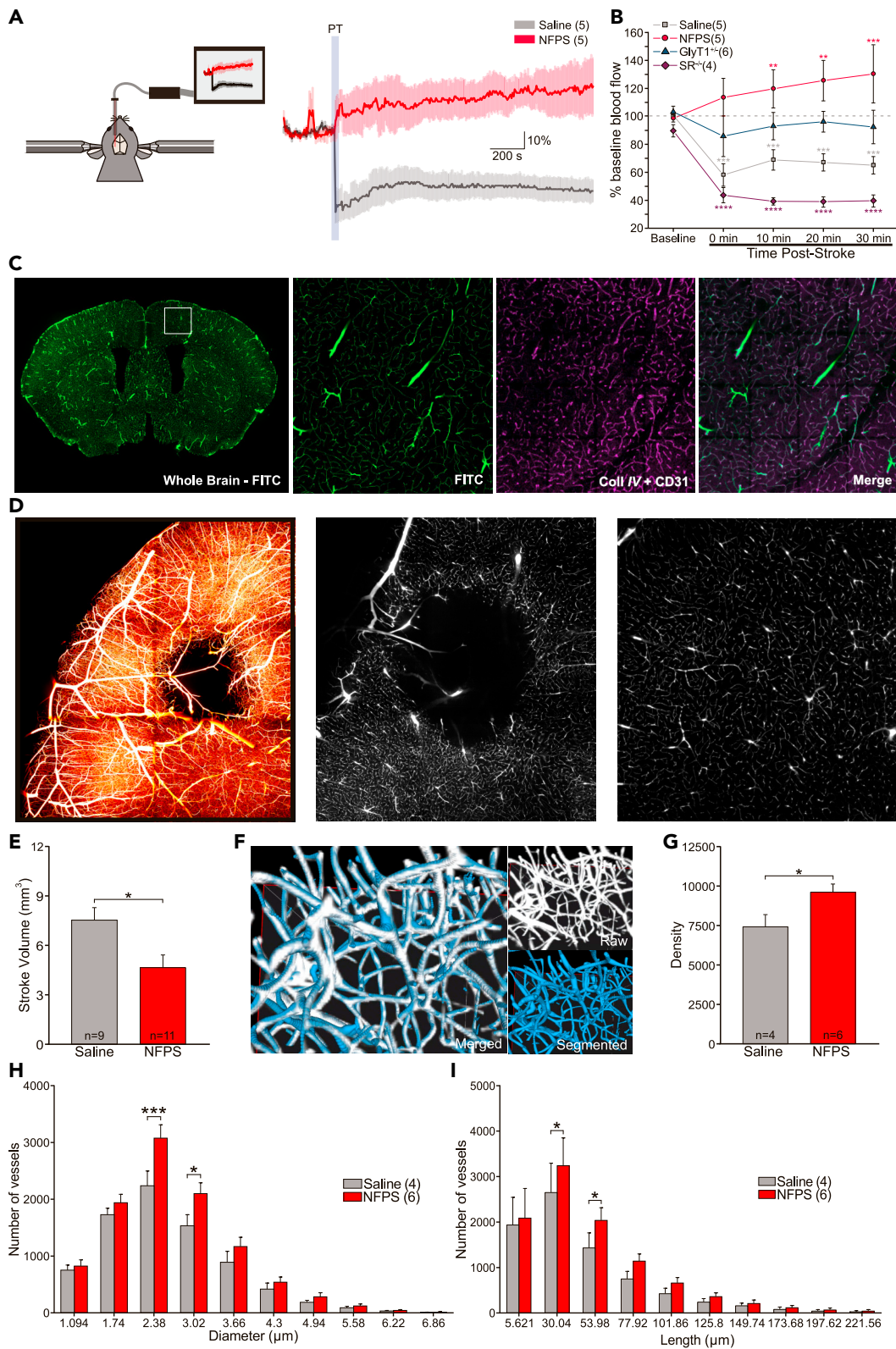


Figure 4. Laser doppler flowmetry blood flow and automatic segmentation of vascular data with AIVIA 9

- (A) Diagram depicting laser doppler flowmetry set-up and the measured effect of NFPS on cerebral blood flow following photothrombotic (PT) stroke.
- (B) Time course of post-stroke cerebral blood flow following PT in mice with varying levels of glycine or D-serine.
- (C) 50 µm coronal section of brain perfused with FITC-BSA. Magnified images from the sensorimotor cortex demonstrating exact colocalization of FITC-BSA perfusion (green) with CD31 and CollIV vascular immunostaining (purple).
- (D) Colored max projection of stroked hemisphere, and single section of raw images depicting vasculature at the stroke and below the stroke, acquired with a light sheet microscope 48hrs following PT stroke.
- (E) Stroke volume bar graph in saline- or NFPS-treated mice, calculated by an automated deep learning prediction model.
- (F) Merged image demonstrating exact colocalization of AIVIA's automatic segmentation to raw data.
- (G) Density of vessels in peri-infarct region in saline- or NFPS-treated mice.
- (H and I) Number of vessels in the stroke area according to diameter and to length. Data is mean \pm SEM; statistical significance p < 0.05 *, p < 0.01 **, p < 0.001 ***, and p < 0.0001 ****.

for complete labeling of the cerebral vasculature (Figure 4C; Videos S3 and S4). We first used a deep learning segmentation model to automatically calculate stroke volume from our cleared tissue (Figures 4D, 4E, and S7B; Video S5). We observed a decrease in stroke volume in NFPS-treated mice compared to saline-treated mice (Figure 4E). These results are consistent with data illustrated in Figure 2B. We further explored the effect of NFPS following PT on vascular density. The PT-induced decrease in vascular density was attenuated with NFPS treatment compared to saline-treated mice, in the peri-infarct region (Figures 4F and 4G). Furthermore, NFPS pre-treatment decreased the PT-induced loss in vessels of smaller diameter and length (Figures 4H and 4I) compared to saline-treated mice, in the peri-infarct region. Taken together, treatment with NFPS before an ischemic event protects the function and morphology of the cerebral vasculature.

DISCUSSION

Our results demonstrate that during an ischemic event, not only glutamate but also glycine is released in the extracellular space. In such ischemic conditions, when GlyT1s are antagonized, glycine accumulates in the synaptic cleft, reaches the “set point,” and triggers GINI. This is the first report demonstrating that GINI occurs *in vivo*, provides neuroprotection, and preserves brain vasculature.

Using whole-cell patch-clamp recordings, we generated dose-response curves and we measured the effects of glycine on NMDAR current amplitudes. We observed that application of low concentrations of glycine ($\leq 250 \mu\text{M}$) increased the NMDAR-EPSC amplitudes (Johnson and Ascher, 1987, 1992). Paradoxically, we found that application of high concentrations of glycine ($> 1 \text{ mM}$) significantly reduced the NMDAR-EPSC amplitudes. This internalization of NMDARs has been reported to be triggered by an increase in NMDAR binding to intracellular clathrin/dynamin-dependent endocytic machinery (Nong et al., 2003; Han et al., 2013). Because the role of GlyT1s is to keep glycine concentrations below the saturating level of the GBS on NMDARs (Furukawa and Gouaux, 2003) the relevance of the pivotal work from Salter and co-workers was questioned by several groups. This low synaptic concentration of endogenous glycine is far from the concentration required to trigger GINI (Aragon et al., 1987; Guastella et al., 1992; Smith et al., 1992; Bergeron et al., 1998). As the effect of different doses of glycine on NMDAR-EPSCs appears to match that of the “inverted-U” shaped curve, we investigated the relationship between glycine levels and NMDAR internalization using *in vitro* ischemic paradigms. We report evidence that synaptic NMDARs internalize following elevation of glycine during a train of stimuli during OGD, an *in vitro* model of ischemia (Rossi et al., 2000). Moreover, we show that application of a high concentration of glycine or D-serine not only triggers GINI but also primes NMDARs for GINI. When a high dose is applied and washed off before application of a low dose of one of the co-agonists, GINI is induced.

Interestingly, we demonstrate, *in vivo*, that elevation of extracellular glycine by pharmacological blockade or genetic deletion of GlyT1 resulted in a decreased stroke volume and an attenuation of motor deficits in mice following ischemic stroke induced by PT or ET-1. This was observed when NFPS was administered 24 h pre-stroke, or up to 10 min post-stroke. We also show evidence that GINI, *in vivo*, is directly modulating the GluN1 subunit of NMDAR channel function during ischemic stroke as the effect of NFPS on both stroke volume and behavior is completely abolished when mice are focally infected with a viral vector expressing a non-internalizing GluN1 receptor subunit (AAV-GluN1-A714L) (Han et al., 2013).

The NMDAR co-agonist, glycine, has been previously shown to be neuroprotective in both *in vitro* (Hu et al., 2016) and *in vivo* models of stroke (Chen et al., 2015, 2017, 2020; Zhao et al., 2018; Qin et al., 2019).

However, the mechanism by which glycine affords neuroprotection during stroke *in vivo* remains elusive. Recent work suggests that it is via modulation of intracellular pathways, including the Phosphatase and tensin homolog (PTEN)/protein kinase B (Akt) signaling pathway (Qin et al., 2019; Zhao et al., 2018), or vascular endothelial growth factor receptor 2 (Chen et al., 2020). Glycine is also thought to exert its neuroprotective effects via mediation of non-ionotropic NMDAR function (Chen et al., 2015, 2017; Hu et al., 2016), or by promoting microglial polarization (Liu et al., 2019). Partial agonists at the GBS on NMDARs also afford neuroprotection following an OGD challenge (Stanton et al., 2009) and during MCAO paradigm (Zheng et al., 2017). Pharmacological elevation of brain glycine following NFPS administration potentiates ischemic preconditioning (Pinto et al., 2015) and confers neuroprotection via global activation of ionotropic GlyRs during transient MCAO (Huang et al., 2016). Overall, there are many ways in which glycine has been shown to be neuroprotective, all of which may be occurring in conjunction with GINI. However, here we report for the first time the important role of GlyTs as the blockade of these transporters minimized cell death following an ischemic stroke in an *in vivo* model.

A recent review suggests that glycine and D-serine may be therapeutically beneficial by down regulating NMDARs, such as rodent models of traumatic brain injury and lipopolysaccharide-induced neuroinflammation (Biegon et al., 2018). There is also a growing body of evidence to suggest that extracellular glycine is neuroprotective in several rodent ischemic stroke models (Huang et al., 2016; Zheng et al., 2017; Zhao et al., 2018; Liu et al., 2019; Chen et al., 2020; Yamamoto et al., 2016). Moreover, the level of extracellular glycine appears to be important in stroke outcome. A low level of glycine, corresponding to increased NMDAR activation, appears to be deleterious. In contrast, an elevated level of glycine appears to be neuroprotective (Yao et al., 2012). These latest findings are in agreement with our data. Indeed, the transgenic GlyT1^{+/−} mice, which have high endogenous levels of glycine and consequently a high occupancy of the GBS, are more resistant to PT, whereas the SR^{−/−} mice, which have a low occupancy of the GBS, are more sensitive to PT challenge.

Despite an overwhelming body of evidence from animal studies that implicate NMDARs in neuronal loss (Gotti et al., 1988; Park et al., 1989; Scatton, 1994; Prass and Dirnagl, 1998), all clinical trials of drugs targeting one of the numerous binding sites on NMDARs have failed because of poor tolerance or lack of efficacy (Ikonomidou and Turski, 2002; Lipton, 2004; Kalia et al., 2008). One reason for this may be the difficulty in obtaining a therapeutic degree of NMDAR-blockade that does not interfere with critical NMDAR-dependent functions in neuronal circuits (Kostandy, 2012). The widespread inhibition of NMDAR function is not compatible with baseline synaptic transmission. As such, our data suggest that attention should turn to modulation of NMDAR function during stroke. In this study, we show that GINI is not a direct antagonism of NMDARs but rather a dynamic and reversible phenomenon which dampens NMDAR-mediated excitotoxicity during ischemia while maintaining basal synaptic activity of NMDARs.

The complex vascular network of the brain and its integrity are essential for normal brain function. Following an ischemic event, the delivery of oxygen and nutrients to neurons and glial cells are impaired. Because the brain is highly vulnerable to compromises in blood supply, we investigated the potential impact of NFPS in preserving brain vasculature. It has been previously reported that changes in microvasculature, such as density and diameter, correlate with disease states (Bennett et al., 2017). PT stroke induced a decrease in vascular density in the peri-infarct region. We found that this decrease was attenuated by a pre-treatment with NFPS. Our histogram analysis shows that vessels of 2–3 μm in diameter were the most affected post-stroke. Application of NFPS decreased the size of vessels occluded, suggesting that the peri-infarct region could undergo enhanced vascular remodeling during the recovery period. We cannot conclude that the mechanism underlying this observation is directly linked to GINI. However, increasing the level of endogenous glycine with NFPS protects the vascular network following stroke, and ultimately leads to improved behavior outcomes.

Overall, our data demonstrate that elevation of glycine via blockade of GlyT1s before or shortly after an ischemic event may provide a rationale for the repurposing of currently approved pharmaceuticals with a similar mechanism of action as potential stroke treatments. For example, the glycine reuptake blocker sarcosine is authorized for clinical use in the treatment of schizophrenia at daily doses of 1–2 g per day and is well tolerated in these patients (Gibert-Rahola and Villena-Rodriguez, 2014; Strzelecki et al., 2014, 2015; Amiaz et al., 2015; Lin et al., 2017). Because the chronic administration of GlyT1-As have been proven to be safe, and we observe the most robust neuroprotective effect when GlyT1-As are administered pre-

stroke, we can envisage GlyT1-As to potentially be utilized as a preventative strategy for stroke. As our *in vivo* data demonstrate the pre-clinical efficacy of this class of drugs in minimizing the deficits induced by PT and ET-1 paradigms, and considering that several GlyT1-As have been tested and proven to be safe and well tolerated in human clinical trials (Harvey and Yee, 2013; Shahsavar et al., 2021), GlyT1 should be tested for a new therapeutic for ischemic stroke.

Limitations of the study

There were limitations to the present study. Although we focused on GINI and concluded that it occurs *in vivo*, we did not investigate how this finding integrated with other known mechanisms of glycine in neuroprotection, such as GlyRa activation. However, we have no reason to believe that GINI could not take place in addition to other mechanisms. Furthermore, although we did not present imaging of GINI occurring *in vivo*, we inferred it occurred based on electrophysiological recordings in acute slices and behavioral experiments. Imaging this phenomenon *in vivo* would be interesting to investigate in future studies. Finally, we did not investigate the mechanism by which NFPS ameliorated post-stroke vasculature as it will be the focus of future work.

ABBREVIATIONS

AAV	Adeno associated virus;
ACSF	Artificial cerebrospinal fluid;
CHO	Chinese Hamster Ovary;
CPA	Cyclopiazonic acid;
CV	Cresyl violet;
DBP	Dynamin blocking peptide;
ddH ₂ O	Double distilled water;
EPSCs	Excitatory postsynaptic currents;
ET-1	Endothelin-1;
FJC	FluoroJade C;
GBS	Glycine binding site;
GINI	Glycine-induced NMDAR internalization;
GluN2A ^{-/-}	NMDAR GluN2A subunit knockout;
GlyR	Glycine receptor;
GlyT1	Glycine transporter type 1;
GlyT1 ^{+/−}	Heterozygous glycine transporter type 1;
GlyT1-A	Glycine transporter type 1 antagonist;
GO	Glycine oxidase;
i.p.	Intraperitoneal;
LDF	Laser Doppler flowmetry;
LSFM	Light sheet fluorescence microscopy;
tMCAO	Transient middle cerebral artery occlusion;
MRI	Magnetic resonance imaging;
NFPS	N-[3-(4'-fluorophenyl)-3-(4'-phenylphenoxy)propyl]sarcosine;
NMDAR	N-methyl-D-aspartate receptor;
NMDG	N-methyl-D-glucamine;
OGD	Oxygen-glucose deprivation paradigm;
PBSG	0.25% (w/v) gelatin in PBS;
PBSGT	0.25% (w/v) gelatin and 0.2% Triton X-100 (v/v) in PBS;
PFA	Paraformaldehyde;
P _{open}	Open probability;
PT	Photothrombosis;
RT	Room temperature;
SR ^{-/-}	Serine racemase knockout;
TTC	2,3,5-triphenyltetrazolium chloride;
VGAT	Vesicular GABA transporter;
VGlut	Vesicular glutamate transporter;
WT	Wild type.

STAR METHODS

Detailed methods are provided in the online version of this paper and include the following:

- KEY RESOURCES TABLE
- RESOURCE AVAILABILITY
 - Lead contact
 - Materials availability
 - Data and code availability
- EXPERIMENTAL MODEL AND SUBJECT DETAILS
 - Animals
 - Cell lines
- METHOD DETAILS
 - Electrophysiology
 - Sniffer-patch technique and OGD paradigm
 - Surgical procedures
 - A714L generation, imaging, and *in vivo* spread quantification
 - Immunofluorescence, stroke volume quantification and cell death assay
 - Tissue clearing light sheet microscopy
 - Behavioural tests
- QUANTIFICATION AND STATISTICAL ANALYSIS
 - Quantification and statistical analysis

SUPPLEMENTAL INFORMATION

Supplemental information can be found online at <https://doi.org/10.1016/j.isci.2021.103539>.

ACKNOWLEDGMENTS

Supported by operating grants from Canadian Institutes of Health Research (MOP-102501) and Heart and Stroke Foundation (G-16-00014016) awarded to Richard BERGERON. Supported also in part by Recherches Neuro-Hippocampe. We thank Dr. B Lacoste and his research associate Dr. X Toussay for their expertise in supervising and allowing us to use their Laser Doppler flowmeter. We also thank the following colleagues for discussions of the project in the last few years: P Albert, JC Béïque, D Corbett, JT Coyle, RW Greene, A Hakim, M Khacho, B Lacoste, D Lagace, DG Rainnie, G Silasi, and G Tsai. This work was completed at the University of Ottawa's Roger Guindon campus in collaboration with the Ottawa Hospital Research Institute. As of August 31st 2021, R.B. is retired from the Ottawa Hospital Research Institute and the University of Ottawa but continues his commitment to biomedical research. Dr. Bergeron is currently the owner (sole director & shareholder) of Recherches Neuro Hippocampe (RNH). RNH provided financial support to the research on the role of glycine in neurotransmission. However, RNH has no investment nor financial interests in any pharmaceutical companies. The financial contribution of RNH was done on a philanthropic basis. Dr. Bergeron's current corresponding address is 1600 Carling Avenue, Suite 100 Ottawa, ON and his current email address is: rbergeron1003rb@icloud.com.

AUTHOR CONTRIBUTIONS

Performed and analyzed electrophysiological experiments: P.K., B.W., W.B., A.Y.C.W., S.R. Purified and determined activity of glycine oxidase: N.A. Carried out behavioral testing and surgical procedures: J.C., A.Y.C.W., A.S., P.K., B.W. Performed immunohistochemistry experiments: J.C., A.S., A.Y.C.W. Generated all molecular biology reagents: P.C. Prepared cleared brain samples: J.C. Constructed and operated the light sheet microscope: B.W., and J.P. Analyzed data imaged with the light sheet microscope: B.W., J.P., J.W. Performed and analyzed laser doppler flowmetry recordings: J.C., and A.Y.C.W. Provided and facilitated access to essential infrastructure: R.B. Supervised the study, performed experimental design and provided scientific direction: R.B. All authors provided advice on data interpretation and critical edits to the text and approved the final manuscript.

DECLARATION OF INTERESTS

We have no competing interest to declare.

INCLUSION AND DIVERSITY

We worked to ensure sex balance in the selection of non-human subjects. One or more authors self-identifies as an underrepresented ethnic minority in science, or as living with a disability. While citing references scientifically relevant for this work, we also actively worked to promote gender balance in our reference list.

Received: July 13, 2021

Revised: October 6, 2021

Accepted: November 24, 2021

Published: January 21, 2022

REFERENCES

- Allen, T.G. (1997). The 'sniffer-patch' technique for detection of neurotransmitter release. *Trends Neurosci.* 20, 192–197.
- Amiaz, R., Kent, I., Rubinstein, K., Sela, B.A., Javitt, D., and Weiser, M. (2015). Safety, tolerability and pharmacokinetics of open label sarcosine added on to anti-psychotic treatment in schizophrenia - a preliminary study. *Isr. J. Psychiatr. Relat. Sci.* 52, 12–15.
- Aragon, M.C., Gimenez, C., and Mayor, F. (1987). Stoichiometry of sodium- and chloride-coupled glycine transport in synaptic plasma membrane vesicles derived from rat brain. *FEBS Lett.* 212, 87–90.
- Aubrey, K.R., and Vandenberg, R.J. (2001). NJ[3-(4'-fluorophenyl)-3-(4'-phenylphenoxy)propyl] sarcosine (NFPS) is a selective persistent inhibitor of glycine transport. *Br. J. Pharmacol.* 134, 1429–1436.
- Aubrey, K.R., Rossi, F.M., Ruivo, R., Alboni, S., Bellonchi, G.C., Le Goff, A., Gasnier, B., and Supplisson, S. (2007). The transporters GlyT2 and VIAAT cooperate to determine the vesicular glycinergic phenotype. *J. Neurosci.* 27, 6273–6281.
- Balkaya, M., Krober, J., Gertz, K., Peruzzaro, S., and Endres, M. (2013). Characterization of long-term functional outcome in a murine model of mild brain ischemia. *J. Neurosci. Methods* 213, 179–187.
- Balu, D.T., Basu, A.C., Corradi, J.P., Cacace, A.M., and Coyle, J.T. (2012). The NMDA receptor co-agonists, D-serine and glycine, regulate neuronal dendritic architecture in the somatosensory cortex. *Neurobiol. Dis.* 45, 671–682.
- Basu, A.C., Tsai, G.E., Ma, C.L., Ehmsen, J.T., Mustafa, A.K., Han, L., Jiang, Z.I., Benneyworth, M.A., Fromowitz, M.P., Lange, N., et al. (2009). Targeted disruption of serine racemase affects glutamatergic neurotransmission and behavior. *Mol. Psychiatr.* 14, 719–727.
- Benedek, A., Moricz, K., Juranyi, Z., Gigler, G., Levay, G., Harsing, L.G., Jr., Matyas, P., Szenasi, G., and Albert, M. (2006). Use of TTC staining for the evaluation of tissue injury in the early phases of reperfusion after focal cerebral ischemia in rats. *Brain Res.* 1116, 159–165.
- Bennett, Rachel E., Robbins, Ashley B., Hu, Miwei, Cao, Xinrui, Betensky, Rebecca A., Clark, Tim, Das, Sudeshna, and Hyman, Bradley T. (2017). Tau induces blood vessel abnormalities and angiogenesis-related gene expression in P301L transgenic mice and human Alzheimer's disease. *Proc. Natl. Acad. Sci. U.S.A.* 115, E1289–E1298.
- Benneyworth, M.A., and Coyle, J.T. (2012). Altered acquisition and extinction of amphetamine-paired context conditioning in genetic mouse models of altered NMDA receptor function. *Neuropharmacology* 37, 2496–2504.
- Bergeron, R., Meyer, T.M., Coyle, J.T., and Greene, R.W. (1998). Modulation of N-methyl-D-aspartate receptor function by glycine transport. *Proc. Natl. Acad. Sci. U.S.A.* 95, 15730–15734.
- Biegton, A., Liraz-Zaltsman, S., and Shohami, E. (2018). Stimulation of N-methyl-D-aspartate receptors by exogenous and endogenous ligands improves outcome of brain injury. *Curr. Opin. Neurol.* 31, 687–692.
- Biswas, S., and Barma, S. (2020). A large-scale optical microscopy image dataset of potato tuber for deep learning based plant cell assessment. *Sci. Data* 7, 371.
- Bouet, V., Boulaud, M., Toutain, J., Divoux, D., Bernaudin, M., Schumann-Bard, P., and Freret, T. (2009). The adhesive removal test: a sensitive method to assess sensorimotor deficits in mice. *Nat. Protoc.* 4, 1560–1564.
- Caldinelli, L., Pedotti, M., Motteran, L., Molla, G., and Pollegioni, L. (2009). FAD binding in glycine oxidase from *Bacillus subtilis*. *Biochimie* 91, 1499–1508.
- Chen, Z., Hu, B., Wang, F., Du, L., Huang, B., Li, L., Qi, J., and Wang, X. (2015). Glycine bidirectionally regulates ischemic tolerance via different mechanisms including NR2A-dependent CREB phosphorylation. *J. Neurochem.* 133, 397–408.
- Chen, J., Hu, R., Liao, H., Zhang, Y., Lei, R., Zhang, Z., Zhuang, Y., Wan, Y., Jin, P., Feng, H., and Wan, Q. (2017). A non-ionotropic activity of NMDA receptors contributes to glycine-induced neuroprotection in cerebral ischemia-reperfusion injury. *Sci. Rep.* 7, 3575.
- Chen, Z., Wang, X., Liao, H., Sheng, T., Chen, P., Zhou, H., Pan, Y., Liu, W., and Yao, H. (2020). Glycine attenuates cerebrovascular remodeling via glycine receptor alpha 2 and vascular endothelial growth factor receptor 2 after stroke. *Am. J. Transl. Res.* 12, 6895–6907.
- Choi, J.H., Yu, N.K., Baek, G.C., Bakes, J., Seo, D., Nam, H.J., Baek, S.H., Lim, C.S., Lee, Y.S., and Kaang, B.K. (2014). Optimization of AAV expression cassettes to improve packaging capacity and transgene expression in neurons. *Mol. Brain* 7, 17.
- Cubelos, B., Gimenez, C., and Zafra, F. (2005). Localization of the GLYT1 glycine transporter at glutamatergic synapses in the rat brain. *Cereb. Cortex* 15, 448–459.
- Deng, J., Dong, W., Socher, R., Li, L.-J., Li, K., and Fei-Fei, L. (2009). Imagenet: a large-scale hierarchical image database. *IEEE Conf. Comput. Vis. Pattern Recogn.* 248–255.
- Dojo Soeandy, C., Salmasi, F., Latif, M., Elia, A.J., Suo, N.J., and Henderson, J.T. (2019). Endothelin-1-mediated cerebral ischemia in mice: early cellular events and the role of caspase-3. *Apoptosis* 24, 578–595.
- EHara, A., and Ueda, S. (2009). Application of Fluoro-Jade C in acute and chronic neurodegeneration models: utilities and staining differences. *Acta Histochem. Cytochem.* 42, 171–179.
- Farr, T.D., Liu, L., Colwell, K.L., Whishaw, I.Q., and Metz, G.A. (2006). Bilateral alteration in stepping pattern after unilateral motor cortex injury: a new test strategy for analysis of skilled limb movements in neurological mouse models. *J. Neurosci. Methods* 153, 104–113.
- Forsythe, I.D., Westbrook, G.L., and Mayer, M.L. (1988). Modulation of excitatory synaptic transmission by glycine and zinc in cultures of mouse hippocampal neurons. *J. Neurosci.* 8, 3733–3741.
- Furukawa, H., and Gouaux, E. (2003). Mechanisms of activation, inhibition and specificity: crystal structures of the NMDA receptor NR1 ligand-binding core. *EMBO J.* 22, 2873–2885.
- Gibert-Rahola, J., and Villena-Rodriguez, A. (2014). Glutamatergic drugs for schizophrenia treatment. *Actas Esp Psiquiatr* 42, 234–241.
- Gomeza, J., Hulsmann, S., Ohno, K., Eulenborg, V., Szoke, K., Richter, D., and Betz, H. (2003). Inactivation of the glycine transporter 1 gene discloses vital role of glial glycine uptake in glycinergic inhibition. *Neuron* 40, 785–796.
- Gotti, B., Duverger, D., Bertin, J., Carter, C., Dupont, R., Frost, J., Gaudilliere, B., MacKenzie, E.T., Rousseau, J., Scatton, B., et al. (1988). Ifenprodil and SL 82.0715 as cerebral anti-ischemic agents. I. Evidence for efficacy in models of focal cerebral ischemia. *J. Pharmacol. Exp. Ther.* 247, 1211–1221.

- Guastella, J., Brecha, N., Weigmann, C., Lester, H.A., and Davidson, N. (1992). Cloning, expression, and localization of a rat brain high-affinity glycine transporter. *Proc. Natl. Acad. Sci. U S A* 89, 7189–7193.
- Han, L., Campanucci, V.A., Cooke, J., and Salter, M.W. (2013). Identification of a single amino acid in GluN1 that is critical for glycine-primed internalization of NMDA receptors. *Mol. Brain* 6, 36.
- Harvey, R.J., and Yee, B.K. (2013). Glycine transporters as novel therapeutic targets in schizophrenia, alcohol dependence and pain. *Nat. Rev. Drug Discov.* 12, 866–885.
- Hatfield, R.H., Mendelow, A.D., Perry, R.H., Alvarez, L.M., and Modha, P. (1991). Triphenyltetrazolium chloride (TTC) as a marker for ischaemic changes in rat brain following permanent middle cerebral artery occlusion. *Neuropathol. Appl. Neurobiol.* 17, 61–67.
- Herdon, H.J., Godfrey, F.M., Brown, A.M., Coulton, S., Evans, J.R., and Cairns, W.J. (2001). Pharmacological assessment of the role of the glycine transporter GlyT1 in mediating high-affinity glycine uptake by rat cerebral cortex and cerebellum synaptosomes. *Neuropharmacology* 41, 88–96.
- Hu, R., Chen, J., Lujan, B., Lei, R., Zhang, M., Wang, Z., Liao, M., Li, Z., Wan, Y., Liu, F., et al. (2016). Glycine triggers a non-ionotropic activity of GluN2A-containing NMDA receptors to confer neuroprotection. *Sci. Rep.* 6, 34459.
- Huang, B., Xie, Q., Lu, X., Qian, T., Li, S., Zhu, R., Yu, W., Chen, G., Chen, Z., Xu, X., et al. (2016). GlyT1 inhibitor NFPS exerts neuroprotection via GlyR Alpha1 subunit in the rat model of transient focal cerebral ischaemia and reperfusion. *Cell Physiol. Biochem.* 38, 1952–1962.
- Ikonomidou, C., and Turski, L. (2002). Why did NMDA receptor antagonists fail clinical trials for stroke and traumatic brain injury? *Lancet Neurol.* 1, 383–386.
- Job, V., Marcone, G.L., Pilone, M.S., and Pollegioni, L. (2002). Glycine oxidase from *Bacillus subtilis*. Characterization of a new flavoprotein. *J. Biol. Chem.* 277, 6985–6993.
- Johnson, J.W., and Ascher, P. (1987). Glycine potentiates the NMDA response in cultured mouse brain neurons. *Nature* 325, 529–531.
- Johnson, J.W., and Ascher, P. (1992). Equilibrium and kinetic study of glycine action on the N-methyl-D-aspartate receptor in cultured mouse brain neurons. *J. Physiol.* 455, 339–365.
- Kalia, L.V., Kalia, S.K., and Salter, M.W. (2008). NMDA receptors in clinical neurology: excitatory times ahead. *Lancet Neurol.* 7, 742–755.
- Kannangara, T.S., Eadie, B.D., Bostrom, C.A., Morsch, K., Brocardo, P.S., and Christie, B.R. (2015). GluN2A^{-/-} mice lack bidirectional synaptic plasticity in the dentate gyrus and perform poorly on spatial pattern separation tasks. *Cereb. Cortex* 25, 2102–2113.
- Ke, M.T., Fujimoto, S., and Imai, T. (2013). SeeDB: a simple and morphology-preserving optical clearing agent for neuronal circuit reconstruction. *Nat. Neurosci.* 16, 1154–1161.
- Kermany, D.S., Goldbaum, M., Cai, W., Valentim, C.C.S., Liang, H., Baxter, S.L., McKeown, A., Yang, G., Wu, X., Yan, F., et al. (2018). Identifying medical diagnoses and treatable diseases by image-based deep learning. *Cell* 172, 1122–1123 e9.
- Kirchhausen, T., Macia, E., and Pelish, H.E. (2008). Use of dynasore, the small molecule inhibitor of dynamin, in the regulation of endocytosis. *Methods Enzymol.* 438, 77–93.
- Kleckner, N.W., and Dingledine, R. (1988). Requirement for glycine in activation of NMDA-receptors expressed in Xenopus oocytes. *Science* 241, 835–837.
- Kostandy, B.B. (2012). The role of glutamate in neuronal ischemic injury: the role of spark in fire. *Neurol. Sci.* 33, 223–237.
- Lai, M.M., Hong, J.J., Ruggiero, A.M., Burnett, P.E., Slepnev, V.I., De Camilli, P., and Snyder, S.H. (1999). The calcineurin-dynamin 1 complex as a calcium sensor for synaptic vesicle endocytosis. *J. Biol. Chem.* 274, 25963–25966.
- Lee, C.J., Mannaioni, G., Yuan, H., Woo, D.H., Gingrich, M.B., and Traynelis, S.F. (2007a). Astrocytic control of synaptic NMDA receptors. *J. Physiol.* 581, 1057–1081.
- Lee, J.K., Park, M.S., Kim, Y.S., Moon, K.S., Joo, S.P., Kim, T.S., Kim, J.H., and Kim, S.H. (2007b). Photochemically induced cerebral ischemia in a mouse model. *Surg. Neurol.* 67, 620–625.
- Lin, C.Y., Liang, S.Y., Chang, Y.C., Ting, S.Y., Kao, C.L., Wu, Y.H., Tsai, G.E., and Lane, H.Y. (2017). Adjunctive sarcosine plus benzoate improved cognitive function in chronic schizophrenia patients with constant clinical symptoms: a randomised, double-blind, placebo-controlled trial. *World J. Biol. Psychiatr.* 18, 357–368.
- Lipton, S.A. (2004). Failures and successes of NMDA receptor antagonists: molecular basis for the use of open-channel blockers like memantine in the treatment of acute and chronic neurologic insults. *NeuroRx* 1, 101–110.
- Liu, X., Smith, B.J., Chen, C., Callegari, E., Becker, S.L., Chen, X., Cianfragna, J., Doran, A.C., Doran, S.D., Gibbs, J.P., et al. (2005). Use of a physiologically based pharmacokinetic model to study the time to reach brain equilibrium: an experimental analysis of the role of blood-brain barrier permeability, plasma protein binding, and brain tissue binding. *J. Pharmacol. Exp. Ther.* 313, 1254–1262.
- Liu, R., Liao, X.Y., Pan, M.X., Tang, J.C., Chen, S.F., Zhang, Y., Lu, P.X., Lu, L.J., Zou, Y.Y., Qin, X.P., et al. (2019). Glycine exhibits neuroprotective effects in ischemic stroke in rats through the inhibition of M1 microglial polarization via the NF-κB p65/Hif-1α signaling pathway. *J. Immunol.* 202, 1704–1714.
- Mallorga, P.J., Williams, J.B., Jacobson, M., Marques, R., Chaudhary, A., Conn, P.J., Pettibone, D.J., and Sur, C. (2003). Pharmacology and expression analysis of glycine transporter GlyT1 with [³H]-N-[3-(4'-fluorophenyl)-3-(4'phenylphenoxy)propyl]sarcosine. *Neuropharmacology* 45, 585–593.
- Mangin, J.M., Baloul, M., Prado De Carvalho, L., Register, B., Rigo, J.M., and Legendre, P. (2003).
- Kinetic properties of the alpha2 homo-oligomeric glycine receptor impairs a proper synaptic functioning. *J. Physiol.* 553, 369–386.
- Martina, M., Gorfinkel, Y., Halman, S., Lowe, J.A., Periyalwar, P., Schmidt, C.J., and Bergeron, R. (2004). Glycine transporter type 1 blockade changes NMDA receptor-mediated responses and LTP in hippocampal CA1 pyramidal cells by altering extracellular glycine levels. *J. Physiol.* 557, 489–500.
- Martina, M., B-Turcotte, M.E., Halman, S., Tsai, G., Tiberi, M., Coyle, J.T., and Bergeron, R. (2005). Reduced glycine transporter type 1 expression leads to major changes in glutamatergic neurotransmission of CA1 hippocampal neurones in mice. *J. Physiol.* 563, 777–793.
- Matsumoto, K., Mitani, T.T., Horiguchi, S.A., Kaneshiro, J., Murakami, T.C., Mano, T., Fujishima, H., Konno, A., Watanabe, T.M., Hirai, H., and Ueda, H.R. (2019). Advanced CUBIC tissue clearing for whole-organ cell profiling. *Nat. Protoc.* 14, 3506–3537.
- Metz, G.A., and Whishaw, I.Q. (2009). The ladder rung walking task: a scoring system and its practical application. *J. Vis. Exp.* 1204.
- Molla, G., Motteran, L., Job, V., Pilone, M.S., and Pollegioni, L. (2003). Kinetic mechanisms of glycine oxidase from *Bacillus subtilis*. *Eur. J. Biochem.* 270, 1474–1482.
- Muller, E., Bakkar, W., Martina, M., Sokolovski, A., Wong, A.Y., Legende, P., and Bergeron, R. (2013). Vesicular storage of glycine in glutamatergic terminals in mouse hippocampus. *Neuroscience* 242, 110–127.
- Nong, Y., Huang, Y.Q., Ju, W., Kalia, L.V., Ahmadian, G., Wang, Y.T., and Salter, M.W. (2003). Glycine binding primes NMDA receptor internalization. *Nature* 422, 302–307.
- Nong, Y., Huang, Y.Q., and Salter, M.W. (2004). NMDA receptors are movin. *Curr. Opin. Neurobiol.* 14, 353–361.
- Paoletti, P., Neyton, J., and Ascher, P. (1995). Glycine-independent and subunit-specific potentiation of NMDA responses by extracellular Mg²⁺. *Neuron* 15, 1109–1120.
- Papouin, T., Ladepeche, L., Ruel, J., Sacchi, S., Labasque, M., Hanini, M., Groc, L., Pollegioni, L., Mothet, J.P., and Oliet, S.H. (2012). Synaptic and extrasynaptic NMDA receptors are gated by different endogenous coagonists. *Cell* 150, 633–646.
- Park, C.K., Nehls, D.G., Teasdale, G.M., and McCulloch, J. (1989). Effect of the NMDA antagonist MK-801 on local cerebral blood flow in focal cerebral ischaemia in the rat. *J. Cereb. Blood Flow Metab.* 9, 617–622.
- Pedotti, M., Ghisla, S., Motteran, L., Molla, G., and Pollegioni, L. (2009). Catalytic and redox properties of glycine oxidase from *Bacillus subtilis*. *Biochimie* 91, 604–612.
- Pineiro, R., Pendlebury, S.T., Smith, S., Flitney, D., Blamire, A.M., Styles, P., and Matthews, P.M. (2000). Relating MRI changes to motor deficit after ischemic stroke by segmentation of functional motor pathways. *Stroke* 31, 672–679.

- Pinto, M.C., Lima, I.V., da Costa, F.L., Rosa, D.V., Mendes-Goulart, V.A., Resende, R.R., Romano-Silva, M.A., de Oliveira, A.C., Gomez, M.V., and Gomez, R.S. (2015). Glycine transporters type 1 inhibitor promotes brain preconditioning against NMDA-induced excitotoxicity. *Neuropharmacology* 89, 274–281.
- Prass, K., and Dirnagl, U. (1998). Glutamate antagonists in therapy of stroke. *Restor. Neurol. Neurosci.* 13, 3–10.
- Qin, X., Akter, F., Qin, L., Xie, Q., Liao, X., Liu, R., Wu, X., Cheng, N., Shao, L., Xiong, X., et al. (2019). MicroRNA-26b/PTEN signaling pathway mediates glycine-induced neuroprotection in SAH injury. *Neurochem. Res.* 44, 2658–2669.
- Rosenmund, C., Stern-Bach, Y., and Stevens, C.F. (1998). The tetrameric structure of a glutamate receptor channel. *Science* 280, 1596–1599.
- Rossi, D.J., Oshima, T., and Attwell, D. (2000). Glutamate release in severe brain ischaemia is mainly by reversed uptake. *Nature* 403, 316–321.
- Rossi, D.J., Brady, J.D., and Mohr, C. (2007). Astrocyte metabolism and signaling during brain ischemia. *Nat. Neurosci.* 10, 1377–1386.
- Sakimura, K., Kutsuwada, T., Ito, I., Manabe, T., Takayama, C., Kushiya, E., Yagi, T., Aizawa, S., Inoue, Y., Sugiyama, H., et al. (1995). Reduced hippocampal LTP and spatial learning in mice lacking NMDA receptor epsilon 1 subunit. *Nature* 373, 151–155.
- Scain, A.L., Le Corronc, H., Allain, A.E., Muller, E., Rigo, J.M., Meyrand, P., Branchereau, P., and Legendre, P. (2010). Glycine release from radial cells modulates the spontaneous activity and its propagation during early spinal cord development. *J. Neurosci.* 30, 390–403.
- Scatton, B. (1994). Excitatory amino acid receptor antagonists: a novel treatment for ischemic cerebrovascular diseases. *Life Sci.* 55, 2115–2124.
- Schallert, T., Fleming, S.M., Leasure, J.L., Tillerson, J.L., and Bland, S.T. (2000). CNS plasticity and assessment of forelimb sensorimotor outcome in unilateral rat models of stroke, cortical ablation, parkinsonism and spinal cord injury. *Neuropharmacology* 39, 777–787.
- Settembre, E.C., Dorresteijn, P.C., Park, J.H., Augustine, A.M., Begley, T.P., and Ealick, S.E. (2003). Structural and mechanistic studies on ThiO, a glycine oxidase essential for thiamin biosynthesis in *Bacillus subtilis*. *Biochemistry* 42, 2971–2981.
- Shahsavari, A., Stohler, P., Bourenkov, G., Zimmermann, I., Siegrist, M., Guba, W., Pinard, E., Sinning, S., Seeger, M.A., Schneider, T.R., et al. (2021). Structural insights into the inhibition of glycine reuptake. *Nature* 591, 677–681.
- Smith, K.E., Borden, L.A., Hartig, P.R., Branchek, T., and Weinshank, R.L. (1992). Cloning and expression of a glycine transporter reveal colocalization with NMDA receptors. *Neuron* 8, 927–935.
- Sommer, Clemens J. (2017). Ischemic stroke: experimental models and reality. *Acta Neuropathol.* 133, 245–261.
- Stanton, P.K., Potter, P.E., Aguilar, J., Decandia, M., and Moskal, J.R. (2009). Neuroprotection by a novel NMDAR functional glycine site partial agonist, GLYX-13. *Neuroreport* 20, 1193–1197.
- Strzelecki, D., Szyburska, J., and Rabe-Jablonska, J. (2014). Two grams of sarcosine in schizophrenia - is it too much? A potential role of glutamate-serotonin interaction. *Neuropsychiatr. Dis. Treat.* 10, 263–266.
- Strzelecki, D., Kaluzynska, O., Szyburska, J., Wlazlo, A., and Wysokinski, A. (2015). No changes of cardiometabolic and body composition parameters after 6-month add-on treatment with sarcosine in patients with schizophrenia. *Psychiatr. Res.* 230, 200–204.
- Toussay, X., Tiberi, M., and Lacoste, B. (2019). Laser doppler flowmetry to study the regulation of cerebral blood flow by G protein-coupled receptors in rodents. *Methods Mol. Biol.* 1947, 377–387.
- Traynelis, S.F., Wollmuth, L.P., McBain, C.J., Menniti, F.S., Vance, K.M., Ogden, K.K., Hansen, K.B., Yuan, H., Myers, S.J., and Dingledine, R. (2010). Glutamate receptor ion channels: structure, regulation, and function. *Pharmacol. Rev.* 62, 405–496.
- Tsai, G., Ralph-Williams, R.J., Martina, M., Bergeron, R., Berger-Sweeney, J., Dunham, K.S., Jiang, Z., Caine, S.B., and Coyle, J.T. (2004). Gene knockout of glycine transporter 1: characterization of the behavioral phenotype. *Proc. Natl. Acad. Sci. U S A* 101, 8485–8490.
- Tsai, P.S., Kaufhold, J.P., Blinder, P., Friedman, B., Drew, P.J., Karten, H.J., Lyden, P.D., and Kleinfeld, D. (2009). Correlations of neuronal and microvascular densities in murine cortex revealed by direct counting and colocalization of nuclei and vessels. *J. Neurosci.* 29, 14553–14570.
- Wang, Y., Jin, K., and Greenberg, D.A. (2007). Neurogenesis associated with endothelin-induced cortical infarction in the mouse. *Brain Res.* 1167, 118–122.
- Wolosker, H., Sheth, K.N., Takahashi, M., Mothet, J.P., Brady, R.O., Jr., Ferris, C.D., and Snyder, S.H. (1999). Purification of serine racemase: biosynthesis of the neuromodulator D-serine. *Proc. Natl. Acad. Sci. U S A* 96, 721–725.
- Wu, Q.J., and Tymianski, M. (2018). Targeting NMDA receptors in stroke: new hope in neuroprotection. *Mol. Brain* 11, 15.
- Yamamoto, S., Ohta, H., Abe, K., Kambe, D., Tsukiyama, N., Kawakita, Y., Moriya, M., and Yasuhara, A. (2016). Identification of 1-methyl-N-(propan-2-yl)-N-((2-[4-(trifluoromethoxy)phenyl]pyridin-4-yl)methyl)-1 H-imidazole-4-carboxamide as a potent and orally available Glycine transporter 1 inhibitor. *Chem. Pharm. Bull. (Tokyo)* 64, 1630–1640.
- Yao, W., Ji, F., Chen, Z., Zhang, N., Ren, S.Q., Zhang, X.Y., Liu, S.Y., and Lu, W. (2012). Glycine exerts dual roles in ischemic injury through distinct mechanisms. *Stroke* 43, 2212–2220.
- Yu, C., Wang, J., Peng, C., Gao, C., Yu, G., and Sang, N. (2018). Bisenet: bilateral segmentation network for real-time semantic segmentation. *Proc. Eur. Conf. Comput. Vis. (Eccv)*, 325–341.
- Zhao, D., Chen, J., Zhang, Y., Liao, H.B., Zhang, Z.F., Zhuang, Y., Pan, M.X., Tang, J.C., Liu, R., Lei, Y., et al. (2018). Glycine confers neuroprotection through PTEN/AKT signal pathway in experimental intracerebral hemorrhage. *Biochem. Biophys. Res. Commun.* 501, 85–91.
- Zheng, C., Qiao, Z.H., Hou, M.Z., Liu, N.N., Fu, B., Ding, R., Li, Y.Y., Wei, L.P., Liu, A.L., and Shen, H. (2017). GLYX-13, a NMDA receptor glycine-site functional partial agonist, attenuates cerebral ischemia injury *in vivo* and *in vitro* by differential modulations of NMDA receptors subunit components at different post-ischemia stage in mice. *Front. Aging Neurosci.* 9, 186.

STAR★METHODS

KEY RESOURCES TABLE

REAGENT or RESOURCE	SOURCE	IDENTIFIER
Antibodies		
Rabbit polyclonal anti-CD31	Abcam	Cat#: ab28364; RRID: AB_726362
Rabbit polyclonal anti-Collagen IV	Abcam	Cat#: ab19808; RRID: AB_445160
FluoTag®-X4 anti-GFP, conjugated with Alexa Fluor 647	NanoTag Biotechnologies	Cat#: N0304-AF647-L
Goat Anti-Rabbit IgG H&L (Alexa Fluor® 647)	Abcam	Cat#: ab150079; RRID: AB_2722623
Bacterial and virus strains		
AAV2/9 GluN1 WT and A714L	University of Laval	This paper
NEB stable	NEB	Cat # C3040I
Chemicals, peptides, and recombinant proteins		
Albumin-fluorescein isothiocyanate conjugate, protein bovine (FITC-BSA)	Millipore Sigma	A9771
BAPTA	Thermo Fisher Scientific	B1204
Cyclopiazonic acid (CPA)	Tocris Biosciences	Cat. No. 1235
Cresyl Violet Acetate Working Solution	Electron Microscopy Sciences	26671-1A
D-APV	Tocris Biosciences	Cat. No. 0106
D-Serine	Millipore Sigma	S4250
Dynamin Blocking Peptide	Tocris Biosciences	Cat. No. 1774
Dyng04a	Abcam	ab120689
Dynasore Hydrate	Millipore Sigma	D7693
Endothelin-1 (human, porcine)	Abcam	ab120471
Fluoro-Jade -C	EMD Millipore	AG325-30MG
Glycine	Millipore Sigma	G7126
HIVAC-F4	Shin-Etsu Chemical	HIVAC-F4
Rose Bengal	Tocris Biosciences	Cat. No. 5168
NBQX	Tocris Biosciences	Cat. No. 0373
N-Butyldiethanolamine, ≥98.6%	Sigma-Aldrich	471240
N-Methylnicotinamide	Fisher Scientific	M037425G
N-[3-[(1,1-Biphenyl]-4-yloxy)-3-(4-fluorophenyl)propyl]-N-methylglycine	Tocris Biosciences	Cat. No. 2789
Nimodipine	Millipore Sigma	N149
Picrotoxin	Tocris Biosciences	Cat. No. 1128
Triphenyltetrazolium chloride (TTC)	Sigma-Aldrich	T8877
Deposited data		
Analyzed data	This paper	N/A
Experimental models: Cell lines		
Hamster: Chinese Hamster Ovary (CHO) cells	N/A	CRL-11268
Human: Human Embryonic Kidney (HEK) cells	N/A	CVCL_0045
Experimental models: Organisms/strains		
Mouse: GlyT1 ^{+/−} : C57Bl/6;S129	Dr. Joseph T. Coyle Laboratory (Tsai et al., 2004)	N/A

(Continued on next page)

Continued

REAGENT or RESOURCE	SOURCE	IDENTIFIER
Mouse: SR ^{-/-} : C57Bl/6;S129	Dr. Joseph T. Coyle Laboratory (Benneyworth and Coyle, 2012)	N/A
Mouse: WT: C57Bl/6	Charles River	CR: 027
Mouse: GluN2A ^{-/-} : C57Bl/6	Sakimura et al., 1995	N/A
Oligonucleotides		
NheI/GluNI F AGCTAGCATGAGCACCATGCACCTGCT	This paper	N/A
EcoRV/GluNI R GATATCTCAGCTCCCTATGACGGG	This paper	N/A
GluN1A714L F – 5'P ACAATTACGAGAGGCCCTGGCT GAGGCCATCCA	This paper	N/A
GluN1A714LR – 5'P GCTCTCGTAATTGTGTTTCCATGTGCCG	This paper	N/A
GluN1shres2 F 5'P CCGCAAATTGCTAATTACAG CATCATGAACCTGCGAGAACGCAAGCTGG 3'	This paper	N/A
GluN1shres2 R 5'PTCCCCATCCTCATTGAATTCCACACGGC 3'	This paper	N/A
Recombinant DNA		
SuperEcliptic Phlourin (SEP)-tagged GluN1	Addgene	#23999
GluN2A in pCDNA3.1	This paper	pRB133
pAAV construct GluN1WT shRNA resistant	This paper	pRB 112
pAAV construct GluN1 A714 shRNA resistant	This paper	pRB 131
pCDNA3.1 Construct GluN1 A714L	This paper	pRB 144
His-tagged glycine oxidase (GO)	Cornell University, NY, USA	Dr. Steven Ealick
Software and algorithms		
AlVIA	DRVISION	Version 9
Automated Stroke Volume Analysis	This paper	GitHub Repository: https://github.com/JulianPitney/Glycine_Transporter_1_Antagonist_Provides_Neuroprotection_in_Vivo_Lightsheet_Analysis.git
ImageJ	https://imagej.nih.gov/ij/	v1.52m
IMARIS	Bitplane	v9.2
Lightsheet Acquisition Software	This paper	GitHub Repository: https://github.com/JulianPitney/Lightsheet
OriginPro	OriginLab	v8.5
Prism	GraphPad	v9.1.0
Terastitcher	GitHub Repository: https://abria.github.io/TeraStitcher/	V1.11.10

RESOURCE AVAILABILITY

Lead contact

Further information and requests for resources and reagents should be directed to and will be fulfilled by the lead contact, Julia Cappelli (jcapp082@uottawa.ca).

Materials availability

Plasmids generated in this study have been deposited to Addgene and will be publicly available as of the date of publication.

Data and code availability

All data reported in this paper will be shared by the lead contact upon request. All original code has been deposited at GitHub and will be publicly available as of the date of publication. DOIs are listed in the [key resources table](#). Any additional information required to reanalyze the data reported in this paper is available from the lead contact upon request.

EXPERIMENTAL MODEL AND SUBJECT DETAILS

Animals

All procedures in this study were carried out on female and/or male 8–10-week-old mice in accordance with the guidelines of the Canadian Council on Animal Care and approved by the University of Ottawa Animal Care Committee. The following transgenic mouse lines were utilized: heterozygous glycine transporter type 1 ($\text{GlyT1}^{+/-}$), serine racemase knockout ($\text{SR}^{-/-}$), and N-methyl-D-aspartate receptor (NMDAR) GluN2A subunit knockout ($\text{GluN2A}^{-/-}$) mice ([Kannangara et al., 2015](#)), along with their wild type (WT) litter mates (on C57Bl/6;S129, C57Bl/6;S129 and C57Bl/6 backgrounds respectively). *In vivo* behavioural experiments were performed on C57Bl/6 WT mice from Charles River ®. The animals were housed under standard conditions and had access to chow and water *ad libitum*.

Cell lines

Cell culture, imaging, and electrophysiological experiments were carried out on Human Embryonic Kidney (HEK293) cells. Sniffer-patch experiments were performed on Chinese Hamster Ovary (CHO) cells. Please see the following sections for more information on maintenance and experimental methods.

METHOD DETAILS

Electrophysiology

Whole-cell electrophysiology on hippocampal slices and HEK293 cells. Whole-cell voltage-clamp recordings were obtained from visually identified CA1 pyramidal cells from acute hippocampal brain slices (300 μm thick) in oxygenated artificial cerebrospinal fluid (ACSF) as previously described ([Martina et al., 2004, 2005](#)). The cells were voltage-clamped at -65 mV using cesium methane sulfonate based internal solution and postsynaptic currents were evoked by electrical stimulation of the Schaffer collaterals with a bipolar stimulating electrode positioned in the *stratum radiatum*. The intensity of the stimulation was adjusted to obtain evoked excitatory postsynaptic currents (EPSCs). The stimulation protocol consisted of a single 100 μs current pulse (10–200 μA) evoked every 12s. For the train stimulation protocol, 10 current pulses (100 μs long) were evoked at 50 Hz for 200 ms and then repeated once every 20s. To isolate the NMDAR-EPSC, a low concentration of MgCl_2 (0.13 mM) ACSF was used wherein the CaCl_2 concentration was increased to 3.5 mM to maintain cation balance.

HEK293 cells were used for electrophysiology recordings 48–72hrs following transfection with either the pHuorin-GluN1-WT or pHuorin-GluN1-A714L cDNA along with an equimolar ratio of the GluN2A. NMDAR currents were evoked using pressure ejection (10psi) from a picospritzer micropipette filled with 10 μM glycine and 1 mM glutamate (Sigma-Aldrich) for a duration of 25–50 ms every 20s at a membrane potential of -60 mV. HEK293 cells were recorded in HEPES-buffered saline external solution with low MgCl_2 using a potassium gluconate recording solution.

When required, additional drugs were applied including various concentrations of D-serine and glycine (Millipore Sigma), as well as 300 nM N-[3-(4'-fluorophenyl)-3-(4'-phenylphenoxy)propyl]sarcosine (NFPS; Tocris Bioscience), 10 mM BAPTA (Thermo Fisher), 30 μM cyclopiazonic acid (CPA) (Tocris Bioscience), and 20 μM nimodipine (Millipore Sigma). The inhibitors of clathrin-mediated endocytosis, 100 μM dynasore (Millipore Sigma), 100 μM dynamin blocking peptide (DBP; Tocris Bioscience), and 30 μM Dyngo4a (Abcam) were included in the internal solution.

Sniffer-patch technique and OGD paradigm

Sniffer-patch technique. To detect glycine release, we used the “sniffer patch” technique ([Allen, 1997](#); [Lee et al., 2007a](#); [Aubrey et al., 2007](#); [Scain et al., 2010](#)). A Chinese Hamster Ovary (CHO) cell line stably

transfected with the 1 alpha 2 subunit of glycine receptor (GlyR) was generated (Mangin et al., 2003). Outside-out membrane patches were excised from the CHO cells using thick-walled borosilicate glass pipettes filled with a cesium chloride internal solution. Following patch excision, the electrode was placed in the stratum radiatum of the CA1 region of the hippocampus to detect glycine release and allow channel activation. Channel open probability (P_{open}) was derived by measuring the mean open time of all the single channel events during the recording window, then dividing by the sum of the mean open and shut times. Multiple channel openings were set as a $P_{open} = 1$ for that particular time period.

Oxygen-glucose deprivation paradigm. To mimic ischemia, the acute slices were challenged by an oxygen-glucose deprivation paradigm (OGD) modified from Rossi et al. (Rossi et al., 2000). In this paradigm, external glucose was replaced with 7 mM sucrose, and the external solution was saturated with 95% N₂/5% CO₂ instead of 95% O₂ / 5% CO₂. Iodoacetate and cyanide were also added to the OGD external solution to block glycolysis and oxidative phosphorylation.

Purification of glycine oxidase. The plasmid containing His-tagged glycine oxidase (GO) was generated from *Bacillus subtilis*. This plasmid was a gift from Dr. Steven Ealick (Cornell University, NY, USA). The protein was expressed in *E. coli* and purified as previously described (Job et al., 2002; Settembre et al., 2003; Molla et al., 2003; Pedotti et al., 2009; Caldinelli et al., 2009).

Surgical procedures

Photothrombosis and endothelin-1 stroke. NFPS or a vehicle control solution was injected intraperitoneally (*i.p.*) into C57Bl/6 mice either 24hrs prior to stroke or 10mins/60mins/120mins post-stroke, at a dose of 5 mg/kg. Photothrombotic (PT) (Lee et al., 2007b) or cortical endothelin-1 (ET-1) (Wang et al., 2007) strokes were induced as previously described. Mice were anesthetized with 2.5% isoflurane in O₂ and mounted onto a stereotaxic frame. For PT strokes, a dose of 10 mg/mL of Rose Bengal (Tocris) was injected *i.p.*. Immediately following the injection of the dye, the skull was exposed to visualize bregma. Using the stereotaxic device, a 520 nm laser (~20 mW; Beta Electronics) was positioned above the sensorimotor cortex (AP+0.7, ML+2.0) and turned on for 10mins to induce a permanent occlusion. For ET-1 strokes, once the skull was exposed and a craniotomy performed for each injection site (1. AP +0.0, ML +2.0, DV -1.6; 2. AP +0.2, ML +2.0, DV -1.4; 3. AP +0.4, ML +2.0, DV-1.3), 1 μL of 2 μg/μL human, porcine ET-1 (Abcam), dissolved in 2.7 μg/μL L-NAME (Abcam), was injected over 5mins with a 28G 10 μL Hamilton syringe to induce a transient ischemic stroke.

Cortical infection with AAVs. Mice were anesthetized with 2.5% isoflurane in O₂ and mounted onto a stereotaxic apparatus. The intact skull was exposed to visualize bregma. The following injection sites were measured from bregma: 1. AP +1.2, ML +2.0, DV -0.5; 2. AP +0.2, ML +2.0, DV -0.5. A craniotomy was performed at each site prior to injecting 0.5 μL of 10⁻¹² PFU/mL (plaque forming units) of either a AAV-WT-GluN1 or the mutant AAV-GluN1-A714L construct, over 5mins with a 28G 10 μL Hamilton syringe. Please refer to section entitled "Generation of WT and A714L viral constructs", below, for more information.

Laser Doppler Flowmetry. Laser Doppler Flowmetry (LDF) recordings following PT were performed as previously described (Toussay et al., 2019). Mice were anesthetized with an *i.p.* injection of a 0.01 ml/g cocktail consisting of 120 mg/kg ketamine and 10 mg/kg xylazine, and then mounted onto a stereotaxic apparatus. Following exposure and thinning of the skull, the laser probe (Transonic Systems) was positioned over the sensory motor cortex (AP +0.7, ML +2.0) and baseline activity was recorded for 5 mins. The laser probe was replaced with a 520 nm laser (~20 mW; Beta Electronics) to induce PT stroke, as described above. Following PT, LDF recordings were performed for an additional 30 mins.

A714L generation, imaging, and *in vivo* spread quantification

Generation of WT and A714L viral constructs. The GluN1 constructs were made by cloning the GluN1 coding region of a SuperEcliptic Phluorin (SEP)-tagged GluN1 construct (Addgene #23999) (Choi et al., 2014) into pDrive cloning vector (pDrive cloning vector, Qiagen). We then used this as a template to create the A714L mutant clone by site-directed mutagenesis. These cDNAs were used for transfection of HEK293 cells. For generation of GluN1-WT and GluN1-A714L adeno-associated virus (AAV), the coding fragments of these constructs were sub-cloned into an adeno-associated viral vector, and viral constructs were then packaged with plasmid AAV2/9 at the University of Laval.

NMDAR internalization imaging in HEK293 cells. HEK293 cells were transiently transfected with either pHluorin-GluN1-WT or pHluorin-GluN1-A714L cDNAs together with GluN2A cDNA. HEK293 cells were then grown for 24-48hrs in the presence of D-APV (Tocris Bioscience). Images were acquired with an LSM880 Confocal Microscope (Zeiss), with cells in a modified HEPES buffer (add 1 mM Glutamate, omit 0.13 mM MgCl₂). A 647 nm-tagged FluoTag®-X4 anti-GFP (1:250-1:500; NanoTag Biotechnologies) was added to tag extracellular NMDARs prior to the acute application of an internalizing dose of glycine. The nanotags (anti-GFP nanobody) are cell impermeable and tag NMDARs on the cell surface. Therefore, the nanotags were observed within the cell only when NMDARs had been internalized. Images were acquired every 3mins over 10-12mins to visualize internalization. Internalization was deemed to have occurred when the cell-impermeable NanoTag (647) was observed within the cell.

Viral spread quantification. Three weeks following cortical infection, mice were transcardially perfused with 1X PBS, followed by 4% PFA. Brains were sliced into 0.5 mm coronal slices and cleared following the SeeDB tissue clearing protocol described by Ke et al. (Ke et al., 2013). Following tissue clearing, brains were imaged with the Zeiss LSM800 confocal microscope. All viral spread analysis was performed manually using Fiji.

Immunofluorescence, stroke volume quantification and cell death assay

Immunohistochemistry. Antigen retrieval was performed on slices before being washed then permeabilized with 0.25% (w/v) gelatin and 0.2% Triton X-100 (v/v) in PBS (PBS-GT). Slices were incubated in primary antibodies in PBS-GT, then washed three times with PBS-GT before the addition of fluorescent secondary antibodies at room temperature (RT). Slices were rinsed, air-dried, and mounted onto slides (Table S1) (Muller et al., 2013). Platelet endothelial cell adhesion molecule-1 (CD-31; 647 nm) and Collagen IV (CollIV; 647 nm) were depicted in purple and visually colocalized to filled, perfused vessels (488 nm).

Quantification of stroke volume — magnetic resonance imaging. Magnetic resonance imaging (MRI) was performed at the University of Ottawa pre-clinical imaging core using a 7 Tesla GE/Agilent MR 901. Mice were anaesthetized for the MRI procedure using isoflurane in O₂: induction at 3%, maintenance at 1.5%. A 2D fast spin echo sequence (FSE) pulse sequence was used for the imaging, with the following parameters: slice thickness = 0.5 mm, spacing = 0 mm, field of view = 2.5 cm, matrix = 256 x 256, echo time = 41 ms, repetition time = 7000 ms, echo train length = 8, bandwidth = 16 kHz, fat saturation. Stroke lesions demonstrated hyperintensity.

Quantification of stroke volume — triphenyltetrazolium chloride. Stroke volume quantification was performed using 2,3,5-triphenyltetrazolium chloride (TTC; Sigma) (Hatfield et al., 1991; Benedek et al., 2006). Forty-eight hours post-stroke, mice were deeply anesthetized with 5% isoflurane in O₂ before decapitation for slicing on a vibratome (Leica) in cold ACSF at 0.5 mm. Slices were incubated in 2% TTC at 37°C for 10mins, then transferred to 4% paraformaldehyde (PFA) at 4°C. Brain slices were imaged from both sides and the surface area of the infarct regions were measured on Fiji (ImageJ.com) and multiplied by the thickness of the slice to obtain a final volume.

Quantification of stroke volume — cresyl violet. Forty-eight hours post-stroke, mice were transcardially perfused with 1X PBS, followed by 4% PFA. Brains were collected and post-fixed in 4% PFA overnight and then incubated in sucrose until saturation. Serial 25 µm thick coronal sections were cut on a cryostat (Microm HM500), and collected onto positively charged Superfrost Plus Microscope Slides (Fisher Scientific). The slides were immersed in xylene and then rehydrated in decreasing concentrations of ethanol before being placed in double distilled water (ddH₂O). Once rehydrated, slides were stained with cresyl violet (CV) (Electron Microscopy Sciences) and placed in ddH₂O. Slides were then dehydrated in increasing concentrations of ethanol before being immersed in xylene. Once removed, the slides were mounted with DPX mounting media (Sigma). Images of CV-stained slices were acquired with the EVOS FLAuto2 inverted epifluorescence microscope under brightfield. The surface area of the infarct regions was multiplied by the distance between each collected slice (500 µm) to obtain a volume. The sum of all slices was used to obtain a final stroke volume per brain.

Quantification of neuronal loss — FluoroJade C. The brain tissue preparation for FluoroJade C (FJC; EMD Millipore) was treated exactly as that of the CV brain tissue. Slides were first immersed in 1% sodium hydroxide in 80% ethanol, 70% ethanol and finally in ddH₂O before being incubated in a 0.06% potassium

permanganate (Sigma-Aldrich) solution. This was followed by an incubation in a 0.0001% FJC solution dissolved in 0.1% aqueous acetic acid and combined with 0.0001% DAPI (Santa Cruz Biotechnology), and slides were once again rinsed with ddH₂O and left to air dry. Slides were then immersed in xylene and mounted with FluoroMountG (Sigma-Aldrich) (Ehara and Ueda, 2009). Imaging was completed with the Zeiss AxioObserver Z1 inverted epifluorescence microscope using GFP (488/509 nm) and DAPI (359/461 nm) filters. Analysis of the total number of degenerating neurons was performed using IMARIS 9.2 (Bit-plane). IMARIS 9.2 was set to detect and count all green (representing degenerating neurons) and blue (representing nuclear DNA) spots on each image and then calculate colocalization. The cells having been tagged by both DAPI and FJC were counted as FJC positive neurons.

Tissue clearing light sheet microscopy

Tissue clearing. CUBIC tissue clearing was completed as previously described (Matsumoto et al., 2019). Following perfusion, the tissue was post-fixed overnight in 4% PFA, then washed in 1X PBS the following day. Following washes, tissue was submerged in half diluted CUBIC-L (1:1, CUBIC-L:Water) at 37°C overnight. Tissue was submerged in CUBIC-L at 37°C with gentle shaking over 10 days, changing the solution every 48hrs. Tissue was then washed in 1X PBS before being submerged in half diluted CUBIC-R^{+(M)} (1:1, CUBIC-R^{+(M)}:Water) overnight at RT with gentle shaking. Tissue was submerged in CUBIC-R^{+(M)} the following day, then replaced with fresh CUBIC-R^{+(M)} 24hrs later. Tissue was imaged with a light sheet microscope in a refractive index matched imaging solution consisting of a mixture of HIVAC-4 with mineral oil.

Imaging and segmentation. Imaging was performed using our custom-built light sheet microscope. CUBIC-cleared brains were imaged using a 2.5X objective (NA0.07), 488 nm excitation laser line and 5 μm steps. Each sample was scanned as a series of tiles, then stitched into a single image using TeraStitcher. The stitched scans were then run through AIVIA 9 to segment and create 3D reconstructions of the vascular network. Properties of each vessel (diameter and length) were automatically calculated by AIVIA 9, and then exported for analysis.

Automated quantification of stroke volume (stroke volume prediction). Stroke volume in cleared tissue was calculated as follows: the areas representing stroke in each slice were identified, multiplied by their z-depth (thickness), then summed to obtain a total volume. The stroke regions were identified in each slice using a deep convolutional neural network (Kermany et al., 2018; Biswas and Barma, 2020; Yu et al., 2018) which was deemed 98% accurate. The network was first pre-trained on a large data-set (Deng et al., 2009), then further trained using 906 experimental scans.

Post-stroke vascular morphology quantification. For analysis of vascular morphology in the peri-infarct region, transcardial FITC-BSA staining was paired with CUBIC brain clearing to allow for LSFM imaging. Forty-eight hours post PT stroke, mice were transcardially perfused with 20 mL 1X PBS, then 20 mL 4% PFA. Mice were then submerged in a 37°C water bath, facing down at an angle of 30° before being perfused with 10 mL of 0.5% FITC-BSA (Sigma-Aldrich), in 2% gelatin (Sigma-Aldrich). Subsequently, mice were submerged in an ice bath for 30mins before the brain was dissected out (Tsai et al., 2009). Brains were collected and post-fixed in 4% PFA overnight, then cleared following the CUBIC tissue clearing protocol. Following tissue clearing, brains were imaged by LSFM. A 1.125 mm³ region of interest lateral to the stroke site was manually selected, then analyzed using AIVIA 9 (DRVISION Technologies).

Behavioural tests

Adhesive removal test. The adhesive removal test was performed as described (Bouet et al., 2009). Mice were trained pre-stroke daily over 5 days and tested post-stroke over 2 days. Trials began with 1 min of habituation to an empty home cage, before strips of adhesive were placed onto both forepaws. The mouse was then placed back into the cage and the times to contact and remove the adhesive strips were recorded by two experimenters. Mice were allotted a maximum of 2mins to complete the task. The times to contact and remove the pieces of adhesive tapes were compared per paw as well as pre- and post-stroke.

Horizontal ladder test. The horizontal ladder test was performed based on protocols described previously (Farr et al., 2006; Metz and Whishaw, 2009) with slight modifications. Mice underwent one day of training prior to stroke. In the pre-stroke trials, mice crossed the ladder up to seven times or until they had performed two acceptable runs. In turn, during the post-stroke trials, mice had three attempts to cross

the ladder, two of which were scored. Each trial was recorded with a video camera. Scoring and analysis were performed by an experimenter blind to the conditions. The video recordings of the best two trials from each mouse were analyzed frame-by-frame with Noldus Observer XT program. Each limb's step was scored as either "correct", "partial" or "miss". The percentage of missed steps pre- and post-stroke were compared.

Cylinder test. The cylinder test was performed based on protocols described (Schallert et al., 2000; Balkaya et al., 2013), with slight modifications. Mice were placed in a transparent cylinder and filmed with an overhead camera until they reared 22 times. With each rear, three types of behaviours were recorded: (A) right paw is exclusively weight bearing; (B) left paw is exclusively weight bearing; (C) both paws are weight bearing at the same time. The video recordings of each trial were analyzed frame-by-frame with Noldus Observer XT program by a single experimenter blind to the conditions. The length and frequency of fore-limb contacts to the wall of the cylinder were scored. The behaviours were expressed per paw as an average time in relation to the sum of the independent left and right weight bearing. The average time spent on the impaired paw (right) was compared in pre-stroke and post-stroke trials.

QUANTIFICATION AND STATISTICAL ANALYSIS

Quantification and statistical analysis

All data are presented as means \pm S.E.M.; n represents the number of mice or cells in each group, as indicated in each figure. In most cases, statistical significance was determined by a paired, two-tailed Student's t-test or a two-way repeated measure ANOVA followed by Bonferroni post hoc comparisons, for multiple group comparisons. In cases in which datasets had multiple missing values, a mixed-model (ANOVA) was implemented by GraphPad Prism. For analyses of groups across multiple time points, a one-way ANOVA was utilized. Statistical analyses and data presentation were completed using both OriginPro 8.5 (Origin-Lab Software) and GraphPad Prism 8 (GraphPad Software).

For electrophysiological data, decay kinetic and amplitude analysis were performed on averaged traces. Decay time constants were best fit with a double exponential function and expressed as a weighted mean. Due to summation, EPSC amplitudes in the train were measured from the end of the previous EPSC rather than from the initial baseline.

Please refer to [Supplementary methods](#) for more detailed description of all methods.